

PRODUCTION OF VECTOR MESONS BY MUONS IN A
HYBRID BUBBLE CHAMBER EXPERIMENT*

J. Ballam, E.D. Bloom, J.T. Carroll, G.B. Chadwick, R.L.A. Cottrell,
M. Della Negra†, H. DeStaebler, L.K. Gershwin††, L.P. Keller,
M.D. Mestayer, K.C. Moffeit, C.Y. Prescott, S. Stein

Stanford Linear Accelerator Center
Stanford University, Stanford, California 94305

ABSTRACT

We present results on vector meson lepto-production in the SLAC fast cycling 40 inch hydrogen bubble chamber exposed to 16 GeV/c muons. From 3644 inelastic events we obtained 495 events of $\mu^- p \rightarrow \mu^- \pi^+ \pi^- p$ of which approximately 160 are rho events with $W > 2$ GeV and $Q^2 > 0.05$ GeV². Analyzing this data in the same way as in our previous photoproduction experiment, we find the ρ^0 contribution to σ_{TOT} decreases by about 35% between $Q^2 = 0$ and 1 GeV², and the exponential slope parameter becomes approximately 20% smaller, although within errors it is still consistent with the photoproduction value. The decay angular distribution of the ρ^0 shows a substantial $\cos^2\theta$ component which can be interpreted as evidence for production by longitudinal photons assuming s-channel helicity is conserved. Data from 39 ω -production events is also presented. Upper limits for ϕ and ρ' production are given.

(Submitted to Phys. Rev. D)

* Work supported by the U.S. Atomic Energy Commission.

† Present address: CERN, Geneva, Switzerland.

†† Present address: Institute for Defense Analysis, Washington, D.C.

I. INTRODUCTION

Vector meson photoproduction has been shown^{1,2} to be an important contribution to the total γ -p cross section. In the vector dominance model,³ vector meson production is assigned the role of the elastic scattering in hadron-hadron interactions. Since both processes have roughly energy independent cross sections and exponential momentum transfer dependence (with slope parameter $\approx 7 \text{ GeV}^{-2}$), the identification of both with the diffractive process is very reasonable. Furthermore, from the decay angular distributions of photoproduced vector mesons it has been found that s-channel helicity conserving amplitudes and natural parity exchanges in the t-channel are dominant. It is therefore interesting to see how the characteristics of this diffractive process depend upon the "mass" of the incident particle.

In lepto-production the reaction

$$\mu^- p \rightarrow \mu^- + \text{hadrons} \quad (1)$$

proceeds in two steps as illustrated in Fig. 1. These are the exchange of a virtual photon γ_v , of laboratory energy ν and absolute value of mass squared, Q^2 , followed by the reaction

$$\gamma_v p \rightarrow \text{hadrons} \quad (2)$$

with center-of-mass energy squared

$$s = W^2 = M_p^2 + 2 M_p \nu - Q^2.$$

Here M_p is the mass of the proton.

In this paper we report on the Q^2 dependence of the ρ^0 and ω production cross sections and the ρ^0 decay characteristics in the positive Q^2 region of Fig. 1b, where the mass of the photon becomes further from the real vector

meson mass and approaches the "scaling region". We also examine the evidence for production of other vector mesons in this region.

II. EXPERIMENTAL SETUP

We have studied the production of vector mesons by 16 GeV/c muons in the SLAC 40" hydrogen bubble chamber by triggering photographs when the scattered muon is detected. A schematic view of the apparatus is shown in Fig. 2. About 100 muons per pulse passed through the bubble chamber which was expanded 10 times per second. Muons with a scattering angle roughly between 1° and 6° , having an energy greater than 1.4 GeV and penetrating 3 ft. of steel caused a coincidence between two banks of scintillation counter hodoscopes, which provided a fast trigger for the spark chambers. The trajectory of the scattered muon could be found off-line using the spark coordinates recorded on magnetic tape from the measurement by 11 magnetostrictive spark chambers sandwiched between four 12 inch thick pieces of steel. The final decision to trigger the bubble chamber camera lights was made by a PDP-8 computer which checked that the hodoscope hit pattern could have been caused by a track from the HBC fiducial volume. This information, together with the measurement of the tracks on the bubble chamber picture, was used as follows: 1) to remove the contamination by π induced interactions to a level of less than 1% as measured in a separate run with a pion beam, 2) to identify the muon among the fast negatives of the event, 3) to improve the muon momentum measurement by using the analyzing power of the fringe field of the bubble chamber. More details of the experimental apparatus may be found in Ref. (4).

III. RHO-PRODUCTION

The density of the 3644 inelastic events found in this experiment with a matching μ track in the muon telescope is shown as a function of Q^2 and W in

Fig. 3a. From this plot we deduce that the cross sections for specific reactions, expressed as a fraction of the total inelastic cross section, σ_{TOT} , will be meaningful for $Q^2 < 2.5 \text{ GeV}^2$ and $W < 5 \text{ GeV}$. On this plot we show contours of our detection probability, obtained from a Monte Carlo calculation.

To observe "elastic" rho production, we first separate out the relevant channel



A 4C kinematic fit to this hypothesis was tried on all 4 prong events. The resulting χ^2 and the χ^2 -probability distributions are shown in Fig. 4. This shows that the procedures for combining the results of the spark and bubble chamber track information are valid. Here the peak at low probability is compatible with that expected to come from non-gaussian tails of the measured quantities. Therefore a fit was accepted if $\chi^2 < 30$.

A plot of the accepted events from reaction (3) versus Q^2 and W is shown in Fig. 3b. The Q^2 intervals to be used in later analysis are shown here as broken lines. The values are also given in Table I.

In Fig. 3c we plot the $\pi^+ \pi^-$ invariant mass versus W . A distinct ρ^0 signal is evident, with a decreasing background as W increases. We also see that the events below $W = 2 \text{ GeV}$ will have a large background mainly from the $\pi^- \Delta^{++}$ final state. Therefore only events with $W \geq 2 \text{ GeV}$ are used in the following.

Figure 5 shows the $\pi^+ \pi^-$, $p\pi^+$ and $p\pi^-$ invariant mass distributions for events of reaction (3) with $W > 2 \text{ GeV}$ for our chosen Q^2 intervals (the highest Q^2 intervals have been combined here). A strong rho signal is seen in all the plots. In addition, some Δ^{++} (1236) production is observed.

To isolate the contribution of the ρ^0 in reaction (3) the influence of the Δ^{++} and phase space must be taken into account. This was done using a maximum likelihood fit to the Dalitz plot of reaction (3) allowing for contributions from

ρ^0 , Δ^{++} and phase space. The formulae and procedures were the same as those of the SBT collaboration.² Now we describe the results of these fits.

A. Mass Shape

In photoproduction,^{1,2} the ρ^0 mass distribution is skewed with respect to the usual p-wave Breit-Wigner (BW) form. A measure of this mass skewing is obtained by fitting to a form $[M_\rho/M_{\pi\pi}]^n \times \text{BW}(M_{\pi\pi})$, a generalization of the prediction of a diffractive dissociation model by Ross and Stodolsky⁵ (who predicted $n = 4$). While the value found for n in photoproduction events integrated over t is near 4, and the mass spectrum is well described by one value, a strong t -dependence was found; $n = 5.3 \pm 0.3$ for forward produced rhos ($0.02 < |t| < 0.08 \text{ GeV}^2$), with n decreasing linearly with t out to $|t| \sim 0.6 \text{ GeV}^2$ and for $|t| > 0.6 \text{ GeV}^2$ no skewing of the rho mass shape was necessary.² Using a similar model to that of Ross and Stodolsky, Kramer and Quinn⁶ suggest the skewing is both t and Q^2 dependent and predict a skewing factor.

$$\left(\frac{M_\rho^2 + Q^2 + |t|}{M_{\pi\pi}^2 + Q^2 + |t|} \right)^2 \quad (4)$$

which reduces to the Ross-Stodolsky factor at $Q^2 = 0$ and $t = 0$. We note that for forward photoproduced rhos the data already show more skewing than predicted by Eq. (4).

To investigate this effect for $Q^2 > 0$ we have left n as a free parameter in the above fits, which integrate over the t -dependence of the data. We show the resulting values, $\langle n \rangle_t$, in Fig. 6 and Table II. Our results are consistent with the same skewing found in photoproduction. In Fig. 6 we also show the electroproduction results of a similar analysis of Dakin et al.⁷ who concluded that the skewing became less at high Q^2 . Also shown is the Kramer and Quinn prediction for n .⁸ As can be seen in Fig. 6, the two experiments are consistent within errors and both disagree as does photoproduction with the Q^2 dependence of $\langle n \rangle_t$ proposed by Kramer and Quinn. ($\chi^2 = 12.4$ and 15 for 3 degrees of freedom for this experiment and Dakin et al., respectively; both give a confidence level less than 1%.)

B. Cross Sections

The total cross section for inelastic μp scattering as a function of Q^2 and W was determined using a Monte Carlo calculation to provide the probability for detecting the outgoing muon in the trigger system, as is described elsewhere.⁴ To avoid some of the uncertainties in this method, we report here only cross section ratios to the total cross section, given by

$$\frac{\sigma(\gamma_{\nu} p \rightarrow \pi^+ \pi^- p)}{\sigma_{\text{TOT}}} = \frac{\sum_{4C} \omega_i}{\sum_{\text{all}} \omega_i}$$

$$\frac{\sigma(\gamma_{\nu} p \rightarrow \rho^0 p)}{\sigma_{\text{TOT}}} = f(\rho) \frac{\sigma(\gamma_{\nu} p \rightarrow \pi^+ \pi^- p)}{\sigma_{\text{TOT}}}$$

where ω_i is the event weight and $f(\rho)$ is the fraction of ρ^0 found in fitting the unweighted 4C sample in a given Q^2 , W interval to ρ^0 , Δ^{++} and phase space contributions. The channel ratio $\sigma(\gamma_{\nu} p \rightarrow \pi^+ \pi^- p)/\sigma_{\text{TOT}}$ was determined using (a) ω_i equal to the inverse of the detection probability and (b) $\omega_i = 1$. Both methods agree within errors, as would be expected if neither the cross section ratio nor the detection probability vary too strongly over the interval in question. The results of method (a) for the first three Q^2 intervals chosen are given in Table I. The ρ and Δ^{++} fractions in the highest Q^2 bin were determined by estimating the background by hand. We note however that the normalization to σ_{TOT} is based on 75 events in this interval. The radiative corrections to σ_{TOT} given in Table I have been applied to the cross section ratios. The calculated corrections attempt to take into account the radiated photons' effect on the measured Q^2 and W distribution of the events. The errors given in Table I are statistical. All 4-prong events were checked for possible losses of reaction (3) due to radiative effects and systematic biases between the bubble chamber and spark chamber measurements. No measureable losses were found. As upper limits to losses we estimate a systematic uncertainty of +5% and -3%.

To compare these results to photoproduction, we must take account of the variation of $\sigma(\gamma p \rightarrow \pi^+ \pi^- p)/\sigma_{\text{TOT}}$ by about a factor of three across our W interval. This was done by taking the ratio of the average photoproduction cross sections after weighting by the muon event density over the W interval, for $Q^2 > 0.2 \text{ GeV}^2$.

A related problem is that the detection probability for events with $Q^2 < 0.2 \text{ GeV}^2$ is concentrated at W values higher than typical for $Q^2 > 0.2 \text{ GeV}^2$, as can be observed in Fig. 3a. Such events have a muon with sufficiently low energy to be swept out of the beam envelope by the chamber field, and which is therefore detected. Consequently, we have excluded the $Q^2 < 0.2 \text{ GeV}^2$ bin from the comparison of $\sigma(\gamma p \rightarrow \pi^+ \pi^- p)/\sigma_{\text{TOT}}$ and $\sigma(\gamma p \rightarrow \Delta^{++} \pi^-)/\sigma_{\text{TOT}}$ which have a more rapid W-dependence than $\sigma(\gamma p \rightarrow \rho^0 p)/\sigma_{\text{TOT}}$.

In Fig. 7 we give the cross section ratio to total for channel (3), for $\Delta^{++} \pi^-$ and for $\rho^0 p$ as a function of Q^2 , as well as the averaged photoproduction points at $Q^2 = 0$. The importance of both channel (3) and ρ^0 production decreases by $\approx 35\%$ between $Q^2 = 0$ and $Q^2 = 1 \text{ GeV}^2$. Other experiments^{7,9,10} have also found that the ρ^0 virtual photoproduction cross section falls substantially faster than the total cross section as Q^2 increases. However these experiments show a larger falloff of $\sigma(\rho^0)/\sigma_{\text{TOT}}$ than found in this experiment.^{7,10} The different Q^2 dependences may arise from problems connected with:

(1) The variation of the cross section over the large Q^2 and W intervals used.

(2) the determination of $\sigma(\rho)/\sigma_{\text{TOT}}$ at $Q^2 = 0$ for such a large W interval (e.g., $\sigma_\rho/\sigma_{\text{TOT}} \approx 0.185$ and 0.102 at $W = 2$ and 5 GeV , respectively, the extremes of W for this experiment).

(3) A possibly different acceptance probability for rho events versus all, in the normalization to σ_{TOT} .

In order to make the comparison of our experiment to others more precise we have compared our results to a model calculation which removes most of the Q^2 and W dependence. In Table I and Fig. 7c (open circles) we give

$\langle \sigma_\rho \rangle_{\text{VDM}} / \langle \sigma_{\text{TOT}} \rangle_{\text{ep}}$ where

$$\langle \sigma_\rho \rangle_{\text{VDM}} = \frac{(a + b/\sqrt{k}) \exp 6(t_{\min}(Q^2) - t_{\min}(Q^2=0))}{(1 + Q^2/M_\rho^2)^2}$$

$$a = 7.9 \mu\text{b} \quad b = 18.2 \mu\text{b} \cdot \text{GeV}^{1/2}$$

$\langle \sigma_{\text{TOT}} \rangle_{\text{ep}}$ = total cross section from electroproduction¹¹ and the brackets indicate an average over the appropriate Q^2 , W intervals of our experiment. We recognize that $\langle \sigma_\rho \rangle_{\text{VDM}}$ is a crude approximation to the vector dominance model of Sakurai and Schildknecht,¹² but takes into account the large Q^2 variation of the propagator factor and the W dependence of the ρ^0 cross section. The data fall less rapidly with Q^2 than that predicted by the above simple VDM calculation as seen by the open circles in Fig. 7c ($\chi^2 = 13.7$ for 4 degrees of freedom: C.L. $\approx 1\%$). This behavior is expected if the longitudinal component of the photon produces rhos; this component is neglected in $\langle \sigma_\rho \rangle_{\text{VDM}}$ above. To take into account the longitudinal contribution to $\langle \sigma_\rho \rangle_{\text{VDM}}$ vector dominance models^{12, 13} suggest an additional $(1 + \xi^2 \frac{Q^2}{2})$ dependence, where ξ gives the ratio of $\sigma_{\text{L}}(\rho^0 \text{p} \rightarrow \rho^0 \text{p})$ to $\sigma_{\text{T}}(\rho^0 \text{p} \rightarrow \rho^0 \text{p})$. Taking $\xi = 1$ and repeating the calculation for $\langle \sigma_\rho \rangle_{\text{VDM}}$ gives the crosses of Fig. 7c ($\chi^2 = 17.3$ for 4 degrees of freedom: C.L. $< 1\%$). The data lie between the predictions of a vector dominance model with $\sigma_{\text{L}}(\rho^0 \text{p} \rightarrow \rho^0 \text{p}) = 0$ (open circles) and with $\sigma_{\text{L}}(\rho^0 \text{p} \rightarrow \rho^0 \text{p}) = \sigma_{\text{T}}(\rho^0 \text{p} \rightarrow \rho^0 \text{p})$ (crosses). ξ^2 near 0.5 gives a reasonable representation to the Q^2 -dependence of $\sigma(\rho)/\sigma_{\text{TOT}}$. As discussed below in the section on the rho decay angular distributions this inferred longitudinal contribution is consistent with our measured longitudinal rho production.

C. t-Distribution

There is great interest in determining if ρ^0 production by virtual photons becomes less forward peaked at high Q^2 than for photoproduction. However, this is not an easy task for the following reasons:

(1) although for $|t| < 0.6 \text{ GeV}^2$ the photoproduction t-distribution at fixed $M_{\pi\pi}$ is well fit by the form $\exp(At)$,² there is evidence¹⁴ that the distribution becomes flatter for higher $|t|$ — this means the slope parameter A depends on the t interval chosen and experiments with different t ranges cannot be compared directly; (2) the value of A varies across the ρ peak in photoproduction so that the slope is sensitive to the mass interval chosen; (3) at high Q^2 and moderate W, the minimum momentum transfer, t_{\min} , is substantial, and changes with $M_{\pi\pi}$, W, and Q^2 , so that the effective intervals of these quantities are not well defined for large bins.

We note that, probably because of these difficulties, the slopes for ρ photo-production reported in the literature¹⁵ vary from 6 to 9 GeV^{-2} .

To avoid some of the above problems, we have fit the Dalitz plot density for $|t| < 0.6 \text{ GeV}^2$, with a factor e^{At} multiplying the ρ contribution, and have applied the same formulae to the photoproduction and to the present data. This technique avoids the above mentioned difficulties (1) and (3), but since the skewing effect for virtual photons may differ from real photons, (2) remains as an inherent uncertainty. The resulting values of A are given in Fig. 8 and Table II. The slope parameter A is lower by $\sim 20\%$ by $Q^2 = 1 \text{ GeV}^2$, which is consistent with a generally greater decrease reported from other measurements,^{7,9,10} but in our data alone it is also consistent with no change with Q^2 .

D. Decay Angular Distributions

For the description of the ρ^0 decay when produced in the inelastic μ scattering, the usual density matrix representation¹⁶ must be expanded to include

production by longitudinal photons.¹⁷ We use the definitions of Ref. 17. If θ and φ are the polar and azimuthal angles of the π^+ in the ρ^0 rest system (with the z axis along the CMS ρ^0 direction, the x axis in the hadron production plane, and Φ the azimuth of the scattered μ^- with respect to the hadron production plane in the hadronic CMS), then the angular distribution of rho decay is:

$$\begin{aligned}
W(\cos \theta, \phi, \Phi) = & \frac{3}{4\pi} \left[\frac{1}{2} (1 - r_{00}^{o4}) + \frac{1}{2} (3r_{00}^{o4} - 1) \cos^2 \theta - \sqrt{2} \operatorname{Re} r_{10}^{o4} \sin 2\theta \cos \phi \right. \\
& - r_{1-1}^{o4} \sin^2 \theta \cos 2\phi \\
& - \epsilon \cos 2\Phi \left\{ r_{11}^1 \sin^2 \theta + r_{00}^1 \cos^2 \theta - \sqrt{2} \operatorname{Re} r_{10}^1 \sin 2\theta \cos \phi - r_{1-1}^1 \sin^2 \theta \cos 2\phi \right\} \\
& - \epsilon \sin 2\Phi \left\{ \sqrt{2} \operatorname{Im} r_{10}^2 \sin 2\theta \sin \phi + \operatorname{Im} r_{1-1}^2 \sin^2 \theta \sin 2\phi \right\} \\
& + \sqrt{2\epsilon(1+\epsilon+\Delta)} \cos \Phi \left\{ r_{11}^5 \sin^2 \theta + r_{00}^5 \cos^2 \theta - \sqrt{2} \operatorname{Re} r_{10}^5 \sin 2\theta \cos \phi - r_{1-1}^5 \sin^2 \theta \cos 2\phi \right\} \\
& \left. + \sqrt{2\epsilon(1+\epsilon+\Delta)} \sin \Phi \left\{ \sqrt{2} \operatorname{Im} r_{10}^6 \sin 2\theta \sin \phi + \operatorname{Im} r_{1-1}^6 \sin^2 \theta \sin 2\phi \right\} \right] \quad (5)
\end{aligned}$$

where the polarization parameter

$$\epsilon = \frac{1}{1 + \frac{2(Q^2 + \nu^2) \tan^2 \Theta / 2}{Q^2 (1 - Q_{\min}^2 / Q^2)^2}}$$

and $Q_{\min}^2 = 2(EE' - |\vec{p}| |\vec{p}'| - M_\mu^2)$, $\nu = E - E'$, and Θ is the muon scattering angle.

The density matrix elements r_{ij}^α are the same as for polarized photons except

$$r_{ik}^{o4} = \frac{\rho_{ik}^{oT} + (\epsilon + \Delta) R \rho_{ik}^{oL}}{1 + (\epsilon + \Delta) R}, \quad r_{ik}^\alpha = \frac{\rho_{ik}^\alpha}{1 + (\epsilon + \Delta) R} \quad \left| \alpha = 1, 2 \right.$$

where T and L refer to production by transverse and longitudinal photons, respectively. $R = \sigma_L / \sigma_T$ and Δ is defined as, $\Delta = \frac{2M_\mu^2}{Q^2} (1 - \epsilon) \ll 1$. It is clear

that ρ^{oT} and ρ^{oL} can only be separated by varying $\epsilon + \Delta$ at fixed W and Q^2 ; for our data no separation is possible because we had a fixed incident muon energy.

In Fig. 9 we show the angular distribution in $\cos\theta$ and $\Psi = \varphi - \Phi$ for $Q^2 > 0.15 \text{ GeV}^2$ and $W > 2 \text{ GeV}$ for the events in the ρ^o mass region. The data are consistent with isotropy in $\cos\theta$ indicating the presence of longitudinal as well as transverse rho production.

If s-channel helicity conservation (SCHC), found in ρ^o -photoproduction,² is valid for leptoproduction, the $\sin^2\theta$ part of this distribution comes entirely from transversely polarized virtual photons while the $\cos^2\theta$ component measures that from longitudinal photons. Assuming SCHC, the ratio of ρ production by longitudinal photons to that from the transverse photons is

$$R = \frac{\sigma_L(\rho)}{\sigma_T(\rho)} = \frac{1}{\langle \epsilon \rangle} \frac{r_{00}^{o4}}{1 - r_{00}^{o4}}$$

Any anisotropy in the Ψ azimuthal distribution comes from rho production by transverse photons. The Ψ distribution shown in Fig. 9 peaks at 0° and 180° , indicating dominant t-channel natural parity exchange for the transverse beam component, as is found in photoproduction.² In the scatter plot of the same figure, the effect of interference between longitudinal and transverse ρ^o can be seen as enhanced $\Psi = 0^\circ$ (360°) production for $\cos\theta < 0$, and enhanced $\Psi = 180^\circ$ production for $\cos\theta > 0$. A measure of this interference is given by

$$\cos\delta = \sqrt{\frac{2\langle \epsilon \rangle}{r_{00}^{o4}(1 - r_{00}^{o4})}} \left(\text{Re } r_{10}^5 - \text{Im } r_{10}^6 \right)$$

and $\cos\delta = 1$ indicates the amplitudes for the transverse and longitudinal component are in phase.

From the ρ^0 decay angular distribution the values for the density matrix parameters of Eq. 5 were determined from a moment analysis for events in the ρ^0 mass region. For this analysis we used events with $W > 2.5$ GeV and $Q^2 > 0.2$ GeV² in order to eliminate background from the final state $\pi^-\Delta^{++}$. In the 60 events selected we estimate that only ≈ 2 Δ^{++} remain. The values for all parameters are given in Table III.

If s-channel helicity is conserved we expect all density matrix elements of Eq. 5 to be zero except r_{00}^{04} , r_{1-1}^1 , $\text{Im} r_{1-1}^2$, $\text{Re} r_{10}^5$, $\text{Im} r_{10}^6$. Within one to two standard deviations the density matrix elements of Table III are consistent with SCHC with the exception of r_{00}^1 which shows a 2.4 standard deviation effect from zero ($r_{00}^1 > 0$ implies a contribution from single flip helicity amplitudes). We note that in photoproduction ρ_{00}^1 is zero within errors² and r_{00}^1 is also zero within errors in the DESY streamer chamber experiment for $Q^2 > 0$.¹⁰

We assume in the following that SCHC holds in electroproduction as it approximately does in photoproduction and also only natural parity exchange occurs in the t-channel. Then the decay angular distribution of Eq. 5 reduced to

$$W(\theta, \Psi) = \frac{3}{8\pi^2(1 + \epsilon R)} \left[\epsilon R \cos^2 \theta + \frac{1}{2} \sin^2 \theta (1 + \epsilon \cos 2\Psi) - (\epsilon R(1 + \epsilon)/2)^{1/2} \cos \delta \sin 2\theta \cos \Psi \right] \quad (6)$$

We can then determine the two free parameters, R and $\cos \delta$ for finer Q^2 intervals than in Table III by a maximum likelihood fit to the events of reaction (3) with $W > 2$ GeV, accounting for the $\Delta^{++}\pi^-$ and phase space contributions as explained in the discussion of cross section determinations. While only events with $|t| < 0.6$ GeV² were used in the fit, the parameters R and $\cos \delta$ did not

change when all events were used. In Fig. 10 and Table IV we give R and $\cos \delta$ from these fits along with the data of Dakin *et al.*,⁷ and Eckart *et al.*,¹⁰ in the indicated Q^2 intervals. Within errors the experiments agree and show a large contribution of longitudinally polarized rhos which interfere nearly maximally with the transverse component. As discussed in section III.B, vector dominance models^{12, 13} suggest

$$R = \xi^2 \frac{Q^2}{M_\rho^2}$$

where ξ gives the ratio of $\sigma_L(\rho^0 p \rightarrow \rho^0 p)$ to $\sigma_T(\rho^0 p \rightarrow \rho^0 p)$. The measurements (Fig. 10) fall between the two cases: i) $\xi = 1$ with $\sigma_L = \sigma_T$ ¹³ and ii) $\xi \leq 0.35$ suggested by Sakurai and Schildknecht.¹² A similar conclusion was reached in comparing the rho cross section ratio to a vector dominance model calculation (see Fig. 7c).

IV. ω PRODUCTION

In Fig. 11a we plot the $\pi^+ \pi^- \pi^0$ mass distribution from the reaction $\mu^- p \rightarrow \mu^- p \pi^+ \pi^- \pi^0$. The events shown have a 1C fit confidence level greater than 3%, $Q^2 > 0.2 \text{ GeV}^2$ and $W > 2.0 \text{ GeV}$. We observe a clear ω peak. The shaded events have $Q^2 > 0.5 \text{ GeV}^2$ and also show a strong ω peak. While the events plotted have not been weighted by our acceptance, such weighting makes little change in the observed structure. We have estimated the ω cross section by selecting events with $0.74 < M(3\pi) < 0.82 \text{ GeV}$, making a small background correction by hand, and correcting for our 3% probability cut and non- 3π decay modes. In Fig. 11b we plot the ratio $\sigma(\gamma_V p \rightarrow p\omega)/\sigma_{\text{TOT}}$ vs Q^2 for $W > 2.0 \text{ GeV}$. The average values of W and Q^2 for the data in this plot are shown in Table I. Using photoproduction data^{1, 2, 18} we have calculated the ratio $\sigma(\omega)/\sigma_{\text{TOT}}$ at

$Q^2 = 0$ for the same W interval (correcting for the photon energy spectrum). Our data points agree well with the photoproduction value, but do not exclude the Q^2 variation found for $\sigma(\rho)/\sigma_{\text{TOT}}$. Since the ω can be produced by both OPE and diffraction scattering our previous observation of a decrease in the ρ^0 contribution to the total cross section at larger Q^2 need not imply a similar decrease in $\sigma(\omega)/\sigma_{\text{TOT}}$.

For the ω events with $|t| < 0.5 \text{ (GeV/c)}^2$ we find an exponential slope parameter ($\exp(At)$) of $A = 7.5 \pm 1.5 \text{ GeV}^{-2}$. The ω polar and azimuthal angular distributions in the helicity frame, $\cos \theta_H$ and Ψ_H , are consistent with isotropy and are similar to the angular distributions above the ω peak. We find $r_{00}^{04} = 0.20 \pm 0.15$ for ω events with $Q^2 > 0.2 \text{ GeV}^2$. This result is consistent with the photoproduction data.^{1,2,18} We find no evidence for 3-body resonance production other than the ω in the $\pi^+\pi^-\pi^0$ final state. We find about one half the events with $0.8 < M_{\pi^+\pi^-\pi^0} < 1.5 \text{ GeV}$ are associated with Δ^{++} (1236) production. After excluding these events we find no significant A_1 or A_2 production. In the 2-body channels we find a strong Δ^{++} (1236) signal and some weak evidence for Δ^+ and ρ^0 production.

V. ϕ PRODUCTION

We have looked for evidence of ϕ production in the final states corresponding to $\gamma_{\nu}p \rightarrow K^+K^-p$ and $\gamma_{\nu}p \rightarrow K_L K_S p$, with $W > 2 \text{ GeV}$, $Q^2 > 0.2 \text{ GeV}^2$. Only one event ($M_{K^+K^-} = 1024 \text{ GeV}$, $W = 3.3 \text{ GeV}$, $Q^2 = 1.1 \text{ GeV}^2$) is compatible with ϕ production. Using the ratio of $\sigma(\phi)/\sigma_{\text{TOT}}$ found in photoproduction ($0.2 \pm .1\%$ at $W = 2 \text{ GeV}$ to $0.44 \pm .06\%$ at $W = 4.3 \text{ GeV}$) averaged over our virtual photon spectrum as was done for ρ^0 and ω we would expect to have seen $3.3 \pm 1 \phi$ events in this region.

VI. SEARCH FOR HIGHER MASS VECTOR MESON PRODUCTION

Recently evidence for diffractive photoproduction of the ρ' (1600) in the reaction

$$\gamma p \rightarrow \pi^+ \pi^+ \pi^- \pi^- p$$

has been presented.¹⁹ It has been suggested that the higher mass vector mesons may become relatively more important at large Q^2 than the lower mass ρ^0 .¹²

In Fig. 12a we plot the 4π invariant mass against W for events which have $Q^2 > 0.2 \text{ GeV}^2$ and fit the 4-constraint reaction

$$\mu^- p \rightarrow \mu^- \pi^+ \pi^+ \pi^- \pi^- p. \quad (7)$$

The bracket indicates the ρ' region. It is clear that no anomalously large ρ' (1600) signal is present.

In high energy photoproduction, the ρ' signal dominates over background in the 1600 MeV 4π mass region, while for low gamma energies the reverse is true. The division between these two regions is roughly $W = 3 \text{ GeV}$. We therefore take the cross section $\sigma(\gamma_V p \rightarrow p 4\pi)$ for $W > 3 \text{ GeV}$ and $M_{4\pi} < 2 \text{ GeV}$ as an upper limit for ρ' production. In Fig. 12b we show these cross section determinations for two Q^2 bins compared to the photoproduction result with the usual averaging over the γ_V spectrum. These data suggest there is no dramatic change as Q^2 increases.

In photoproduction, an enhancement in the $\pi^+ \pi^- 2\pi^0$ mass spectrum at about 1250 MeV, peaking at small t_{pp} , has been reported.²⁰ A decay mode to $\omega\pi^0$ was favored, and it was suggested that this may be the B meson or possibly a new vector meson $\rho'(1250)$. Such a signal appears as a bump in the mass recoiling against the proton in the reaction

$$\gamma p \rightarrow p \pi^+ \pi^- MM$$

and is enhanced when events are selected with $0.32 < M_{\pi^+\pi^-} < 0.6$ GeV and $|t_{pp}| < 0.5$ GeV². We have searched our data for a possible anomaly in this region using 4-prong events giving no good 1C or 4C fit, thus eliminating the $p\pi^+\pi^-$ and $p\pi^+\pi^-\pi^0$ final states. Figure 13 shows the $\pi^+\pi^- +$ neutrals mass spectrum for $0.2 < Q^2 < 2.5$ GeV² and $W > 3$ GeV. Although the event sample is small, Fig. 13 indicates that the same enhancement may be present for $Q^2 > 0$ with a contribution to σ_{TOT} consistent with that of photoproduction.

CONCLUSIONS

1. We find a distinct ρ^0 signal whose contribution to the total cross section is lower by $\approx 35\%$ at $Q^2 = 1$ GeV² than at $Q^2 = 0$ (Fig. 5 and 7). In the context of a simple vector dominance model the observed ρ fraction requires a contribution to rho muo-production from longitudinal photons as Q^2 increases.
2. The exponential t-dependence is flatter by $\approx 20\%$ at $Q^2 = 1$ GeV than $Q^2 = 0$, although our data does not exclude the possibility of no change in the rho t-dependence as Q^2 increases (Fig. 8).
3. The ρ^0 mass shape is consistent with the skewing found in photoproduction, and does not appear to fit the Q^2 , t-dependence suggested by Kramer and Quinn (Fig. 6).

4. We find that the $\cos \theta$ distribution is no longer $\sin^2 \theta$ in the helicity frame for $Q^2 > 0$. Assuming s-channel helicity conservation holds for $Q^2 > 0$ the $\cos \theta$ distribution suggests a strong contribution from longitudinally polarized rhos. Nearly maximal interference between the longitudinal and transverse amplitudes is observed. (Fig. 9 and 10.)

5. A distinct ω signal is observed for $Q^2 > 0$ which contributes about the same to σ_{TOT} as in photoproduction.

6. No anomalously large production of higher mass vector mesons is observed.

ACKNOWLEDGMENTS

We thank Bob Watt and the bubble chamber operations crew for the operation of the 40 inch HBC at 10 pps without which this experiment would not have been possible. The SLAC accelerator set new records for intensity and energy during our run, which would have been impossible without the enthusiastic support of accelerator operators. Excellent technical assistance was provided by G. Johnson and W. Weeks. The suggestions and help of Professor Yehuda Eisenberg, Dr. Eliezer Kogan, Dr. William Johnson and Dr. Jerry Friedman of SLAC are gratefully acknowledged. Also we thank Kenneth Eynman and Dennis Feick for their help in the data reduction and programming. The careful scanning and accurate measuring efforts of the scanners of CDA and the help of Marie LaBelle was most essential for the success of this experiment. The comments of Dr. Hartwig Spitzer were most helpful.

REFERENCES

1. Cambridge Bubble Chamber Group, Phys. Rev. 146, 994 (1966). Aachen-Berlin-Bonn-Hamburg-Heidelberg-München Collaboration, Phys. Rev. 175, 1669 (1968).
2. SLAC-LBL-Tufts Collaboration, Phys. Rev. D5, 545 (1972), and Phys. Rev. D7, 3150 (1973).
3. J.J. Sakurai, Ann. Phys. (N. Y.) 11, 1 (1960); M. Gell-Mann and A. Zachariasen, Phys. Rev. 124, 953 (1961).
4. J. Ballam, E.D. Bloom, J.T. Carroll, G.B. Chadwick, R.L.A. Cottrell, M. Della Negra, H. DeStaebler, L.K. Gershwin, L.P. Keller, M.D. Mestayer, K.C. Moffeit, C.Y. Prescott, S. Stein, Stanford Linear Accelerator Center Report No., SLAC-PUB-1143 (1973) and E.D. Bloom, XVI International Conference on High Energy Physics, Vol. 2, 66 (1972), National Accelerator Laboratory, Batavia, Illinois; J.D. Jackson and A. Roberts Editors.
5. M. Ross and L. Stodolsky, Phys. Rev. 149, 1172 (1966).
6. A. Kramer and H. Quinn, Nucl. Phys. B55, 222 (1973).
7. J.T. Dakin, G.J. Feldman, W.L. Lakin, F. Martin, M.L. Perl, E.W. Petraske and W.T. Toner, Phys. Rev. Letters 30, 142 (1973).
8. The Kramer-Quinn prediction for the Q^2 dependence of $\langle n \rangle_t$ was obtained by generating at a fixed Q^2 the Breit-Wigner line shape skewed by Eq. 4 at discrete t values. These line shapes were then added together weighted by e^{At} with $A = 6(\text{GeV}/c)^{-2}$. The resulting line shape was then fit to a Breit-Wigner shape skewed by $(M_\rho/M_{\pi\pi})^{\langle n \rangle_t}$ with $\langle n \rangle_t$ determined in the fit.
9. K. Berkelman, XVI International Conference on High Energy Physics, Vol. 4, 41 (1972), National Accelerator Laboratory, Batavia, Illinois.
10. V. Eckardt, H.J. Gebauer, P. Joos, H. Meyer, B. Naroska, D. Notz, W.J. Podolsky, G. Wolf, S. Yellin, H. Dau, G. Drews, D. Greubel, M. Maincke, H. Nagel and E. Rabe, Nucl. Phys. B55, 45 (1973).

11. Private communication W. B. Atwood and S. Stein from their 29 parameter model which accurately describes the electroproduction data for σ_{TOT} over the Q^2 -W range of our experiment.
12. J.J. Sakurai and D. Schildknecht, Phys. Letters 40B, 121 (1972).
13. H. Fraas and D. Schildknecht, Nucl. Phys. B 14, 543 (1969).
14. R. Anderson, D. Gustavson, J. Johnson, D. Ritson, B.H. Wiik, W.G. Jones, D. Kreinick, F. Murphy and R. Weinstein, Phys. Rev. D 1, 27 (1970).
15. K.C. Moffeit, Stanford Linear Accelerator Center Report No., SLAC-PUB-1314 (1973).
16. K. Schilling, P. Seyboth, G. Wolf, Nucl. Phys. B 15, 397 (1970); B 18, 332 (E) (1970).
17. K. Schilling and G. Wolf, DESY Report, DESY 73/13 (1973).
18. J. Ballam, et al., Phys. Rev. Letters 24, 1364 (1970); 26, 155 (E) (1970).
19. H.H. Bingham, et al., Phys. Letters 41B, 635 (1972); M. Davier, et al., Stanford Linear Accelerator Center Report No., SLAC-PUB-1205 (1973).
20. SLAC-Berkeley-Tufts Collaboration; Stanford Linear Accelerator Center Report No., SLAC-PUB-1364 (1973).

TABLE I

Average Q^2 , W , number of events for the Q^2 intervals used. Contribution to σ_{TOT} for $\gamma_V p \rightarrow \pi^+ \pi^- p$, $\gamma_V p \rightarrow \Delta^{++} \pi^-$, $\gamma_V p \rightarrow \rho^0 p$, and $\gamma_V p \rightarrow \omega p$. Columns labelled "radiative correction" gives calculated correction to (σ_{TOT}) . See text for column labelled $\langle \sigma_{\rho}^{>VDM} / \langle \sigma_{TOT} \rangle_{ep}$. Errors are statistical.

| $\gamma p \rightarrow \pi^+ \pi^- p$ | | | | | | | | | |
|--------------------------------------|-------------------------|---|---|---|---|--------------------------------------|--|--|--|
| Q^2 (GeV ²) | $\langle W \rangle$ GeV | Events $\gamma p \rightarrow \pi^+ \pi^- p$ | Radiative Corrections to σ_{TOT} | $\frac{\sigma(\gamma_V p \rightarrow \pi^+ p \pi^-)}{\sigma_{TOT}}$ | $\frac{\sigma_{\Delta^{++}}}{\sigma_{TOT}}$ | $\frac{\sigma_{\rho}}{\sigma_{TOT}}$ | $\frac{\langle \sigma_{\rho}^{>VDM} \rangle}{\langle \sigma_{TOT} \rangle_{ep}}$ * | | |
| 0.05-0.2 | 3.0 | 53 | 0.928 | 0.166 ± 0.025 | -- | 0.135 ± 0.022 | 0.103 | | |
| <0.15 > | | | | | | | | | |
| 0.2 - 0.5 | 2.8 | 109 | 0.951 | 0.173 ± 0.016 | 0.031 ± 0.008 | 0.098 ± 0.013 | 0.087 | | |
| <0.30 > | | | | | | | | | |
| 0.5 - 1.3 | 2.8 | 67 | 0.97 | 0.125 ± 0.015 | 0.015 ± 0.006 | 0.092 ± 0.014 | 0.055 | | |
| <0.77 > | | | | | | | | | |
| 1.3 - 2.5 | 2.8 | 11 | 0.98 | 0.096 ± 0.031 | 0.026 ± 0.013 | 0.06 ± 0.02 | 0.026 | | |
| <1.8 > | | | | | | | | | |

* $\sigma_L(\rho^0 p \rightarrow \rho^0 p) = 0$

| $\gamma p \rightarrow \omega p$ | | |
|---------------------------------|---------------------------|---|
| Q^2 (GeV ²) | $\langle W \rangle$ (GeV) | $\frac{\text{Events } \gamma_V p \rightarrow \omega p}{\sigma_{\omega} / \sigma_{TOT}}$ |
| 0.2 - 0.5 | 2.63 | 18 |
| <0.28 > | | |
| >0.5 | 2.67 | 21 |
| <0.90 > | | |

TABLE II

Exponential slope A and the mass skewing parameter n for rho events with $2 < W < 5$ GeV and $|t_{pp}| < 0.6$ GeV².

| Q^2 (GeV ²) | A (GeV ²) | $\langle n \rangle_t$ |
|---------------------------|-----------------------|-----------------------|
| 0.05 - 0.2 | 6.9 ± 1.5 | 4.25 ± 0.81 |
| 0.2 - 0.5 | 7.1 ± 1.4 | 4.12 ± 0.83 |
| 0.5 - 2.5 | 5.3 ± 1.1 | 4.06 ± 0.94 |

TABLE III

Reaction $\gamma_V p \rightarrow \rho^0 p$ for $Q^2 > 0.2 \text{ GeV}^2$ and $W > 2.5 \text{ GeV}$: Density matrix elements, ratio of longitudinal to transverse ρ^0 production R and interference parameter $\cos \delta$ in the helicity system for $|t| < 0.6 \text{ GeV}^2$ as determined by the method of moments to the events in the ρ^0 mass region ($0.6 < M_{\pi\pi} < 0.9 \text{ GeV}$).

$$\begin{aligned}
 r_{00}^{04} &= 0.33 \pm 0.093 & r_{00}^5 &= 0.068 \pm 0.065 \\
 \text{Re } r_{10}^{04} &= 0.041 \pm 0.057 & r_{11}^5 &= -0.081 \pm 0.047 \\
 r_{1-1}^{04} &= -0.091 \pm 0.083 & \text{Re } r_{10}^5 &= 0.127 \pm 0.039 \\
 r_{00}^1 &= 0.383 \pm 0.16 & r_{1-1}^5 &= 0.120 \pm 0.067 \\
 r_{11}^1 &= -0.033 \pm 0.10 \\
 \text{Re } r_{10}^1 &= 0.20 \pm 0.093 \\
 r_{1-1}^1 &= 0.31 \pm 0.13 \\
 \text{Im } r_{10}^2 &= -0.095 \pm 0.088 & \text{Im } r_{10}^6 &= -0.139 \pm 0.048 \\
 \text{Im } r_{1-1}^2 &= -0.37 \pm 0.12 & \text{Im } r_{1-1}^6 &= 0.0 \pm 0.06
 \end{aligned}$$

$$r_{1-1}^1 - \text{Im } r_{1-1}^2 = 0.68 \pm 0.17$$

$$\text{Re } r_{10}^5 - \text{Im } r_{10}^6 = 0.27 \pm 0.06$$

$$\langle \epsilon \rangle = 0.89$$

$$\cos \delta = +0.76 \pm 0.17$$

$$R = 0.54 \pm 0.23$$

TABLE IV

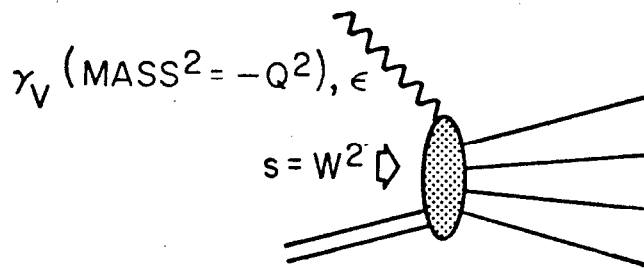
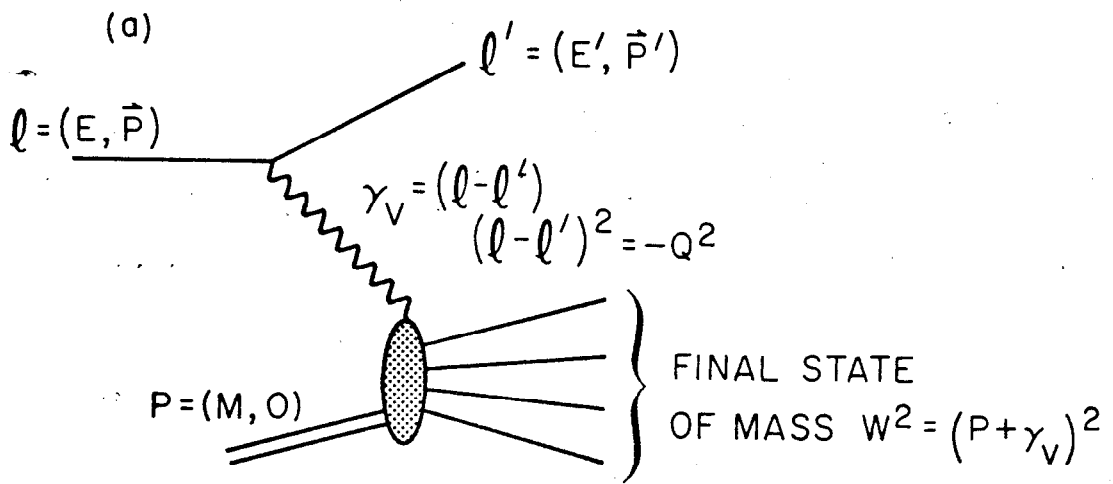
Reaction $\gamma_{\nu} p \rightarrow \rho^0 p$ for $2 < W < 5$ GeV: Parameters R and $\cos \delta$ of Eq. 6 as determined in a maximum likelihood fit.

| Q^2 | R | $\cos \delta$ |
|--------------------|-----------------|-----------------|
| $0.05 < Q^2 < 0.2$ | 0.50 ± 0.25 | 0.34 ± 0.25 |
| $0.2 < Q^2 < 0.5$ | 0.47 ± 0.19 | 0.89 ± 0.17 |
| $Q^2 > 0.5$ | 1.08 ± 0.44 | 0.84 ± 0.19 |

FIGURE CAPTIONS

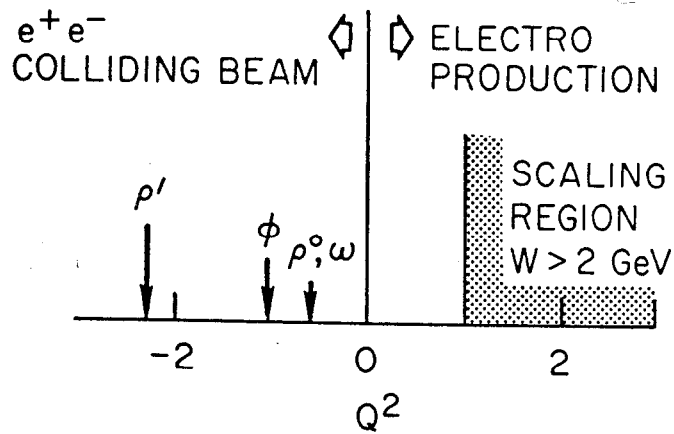
1. (a) Diagram of the scattering process with the variables Q^2 and W defined.
 (b) Domain in the variable Q^2 of electroproduction, photoproduction and colliding beams experiments.
2. Schematic representation of the experiment from the origin of the muon beam to the muon telescope behind the 40-inch hydrogen bubble chamber. The upper part of the figure, depicting the muon beam, is not to scale.
3. (a) Distribution of all events as a function of Q^2 and W . The increased density at large W and low Q^2 is due to larger detection efficiency. Contours displayed are the acceptance probability for the μ -detector. (b) Same for the reaction $\mu^- p \rightarrow \mu^- \pi^+ \pi^- p$. Dashed lines show bins used for ρ^0 analysis. (c) $M_{\pi^+\pi^-}$ versus W . Events not weighted for geometrical acceptance.
4. Chi-squared distribution for the reaction $\mu^- p \rightarrow \mu^- \pi^+ \pi^- p$. Insert shows the χ^2 -probability distribution.
5. Reaction $\gamma_V p \rightarrow \pi^+ \pi^- p$ (a) $\pi^+ \pi^-$ mass distributions for different Q^2 -intervals; (b) same for the $\pi^+ p$ and $\pi^- p$ masses.
6. Q^2 -dependence of the skewing parameter n determined for those events with $|t| < 0.6 \text{ GeV}^2$ for $\gamma_V p \rightarrow \rho^0 p$. Full curve shows the prediction of the model of Kramer and Quinn.
7. (a) ratio of $\gamma_V p \rightarrow \pi^+ \pi^- p / \gamma_V p \rightarrow \text{hadrons}$.
 (b) ratio of $\gamma_V p \rightarrow \pi^- \Delta^{++} / \gamma_V p \rightarrow \text{hadrons}$.
 (c) ratio of $\gamma_V p \rightarrow \rho^0 p / \gamma_V p \rightarrow \text{hadrons}$.
 Photoproduction value from data of SBT collaboration (Ref. 2). Points labelled 0 and x are vector dominance calculations described in the text. Horizontal bars indicate Q^2 intervals used.
8. Q^2 -dependence of the exponential slope A for the reaction $\gamma_V p \rightarrow \rho^0 p$ with $|t_{pp}| < 0.6 \text{ GeV}^2$.

9. Reaction $\gamma_{\nu} p \rightarrow \rho^0 p$ for $Q^2 > 0.15 \text{ GeV}^2$ and $W > 2.0 \text{ GeV}$: Decay angular distribution of events in the ρ^0 region in the helicity system.
10. Reaction $\gamma_{\nu} p \rightarrow \rho^0 p$ for $W > 2.0 \text{ GeV}$: The ratio of longitudinal to transverse ρ^0 production R and cosine of the longitudinal - transverse phase difference $\cos \delta$ assuming s-channel helicity conservation and natural parity exchange in the t-channel. The curves are the predictions of vector dominance models with $\sigma_L = \sigma_T$ (---) and $\sigma_L = 0.35 \sigma_T$ (-.-).
11. Reaction $\gamma_{\nu} p \rightarrow \pi^+ \pi^- \pi^0 p$: (a) $\pi^+ \pi^- \pi^0$ mass distributions. (b) $\sigma(\gamma_{\nu} p \rightarrow \omega p) / \sigma_{\text{TOT}}$.
12. Reaction $\gamma_{\nu} p \rightarrow \pi^+ \pi^+ \pi^- \pi^-$: (top) plot of $\pi^+ \pi^+ \pi^- \pi^-$ mass versus W . (bottom) $\sigma(\gamma_{\nu} p \rightarrow p 4\pi) / \sigma_{\text{TOT}}$ for $W > 3 \text{ GeV}$ and $M_{4\pi} < 2.0 \text{ GeV}$.
13. Reaction $\gamma_{\nu} p \rightarrow p \pi^+ \pi^- + \text{Neutrals}$: $\pi^+ \pi^- + \text{Neutrals}$ invariant mass for $W > 3 \text{ GeV}$. The shaded histograms are those events with $|t_{pp}| < 0.5 \text{ GeV}$ and $0.32 < M_{\pi^+ \pi^-} < 0.6 \text{ GeV}$.



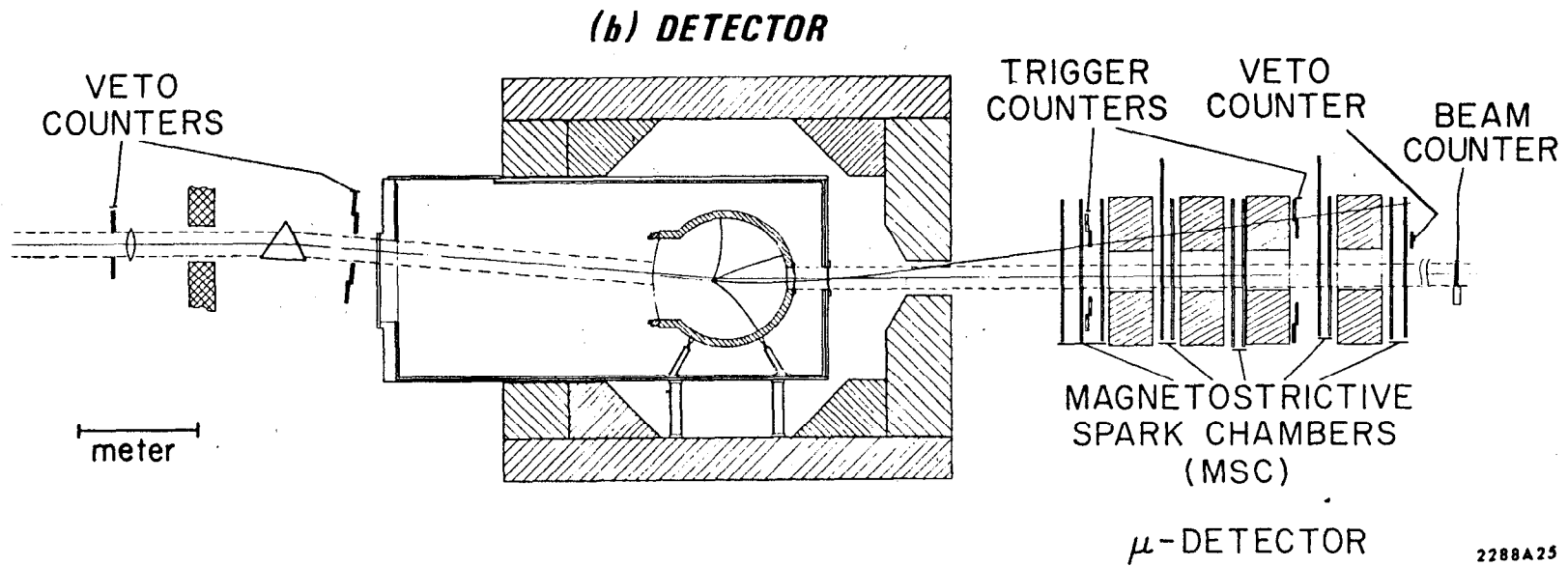
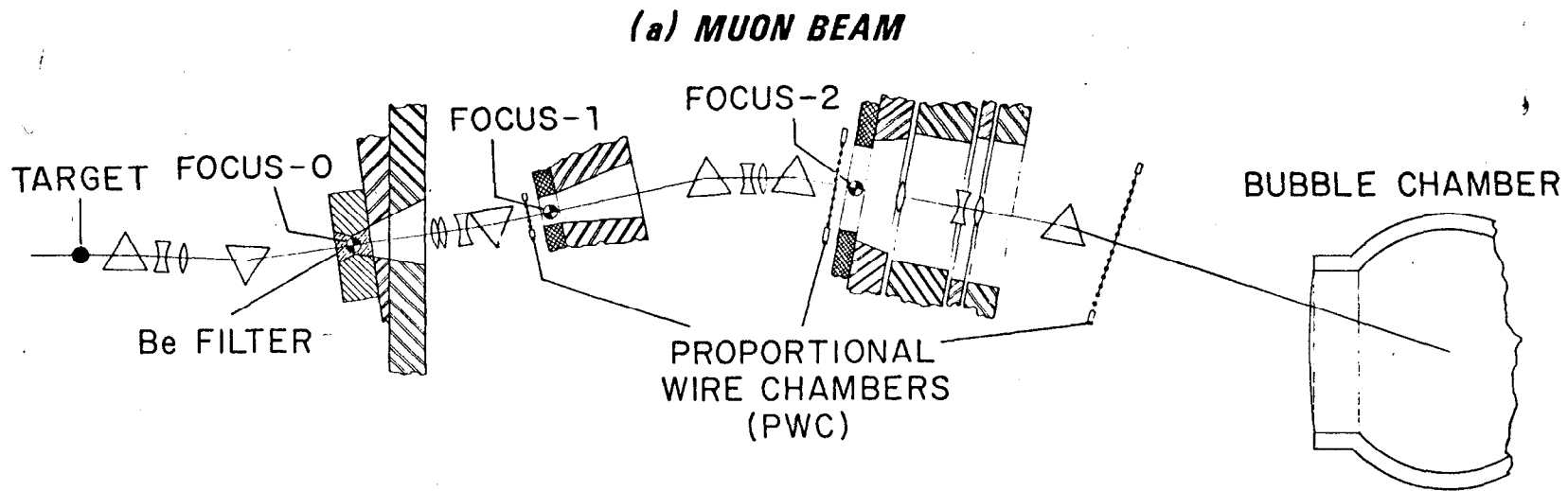
(b)

PHOTO PRODUCTION



2233A12

Fig 1



2288A25

Fig. 2

$\mu^- p \rightarrow \mu^- + \text{anything}$

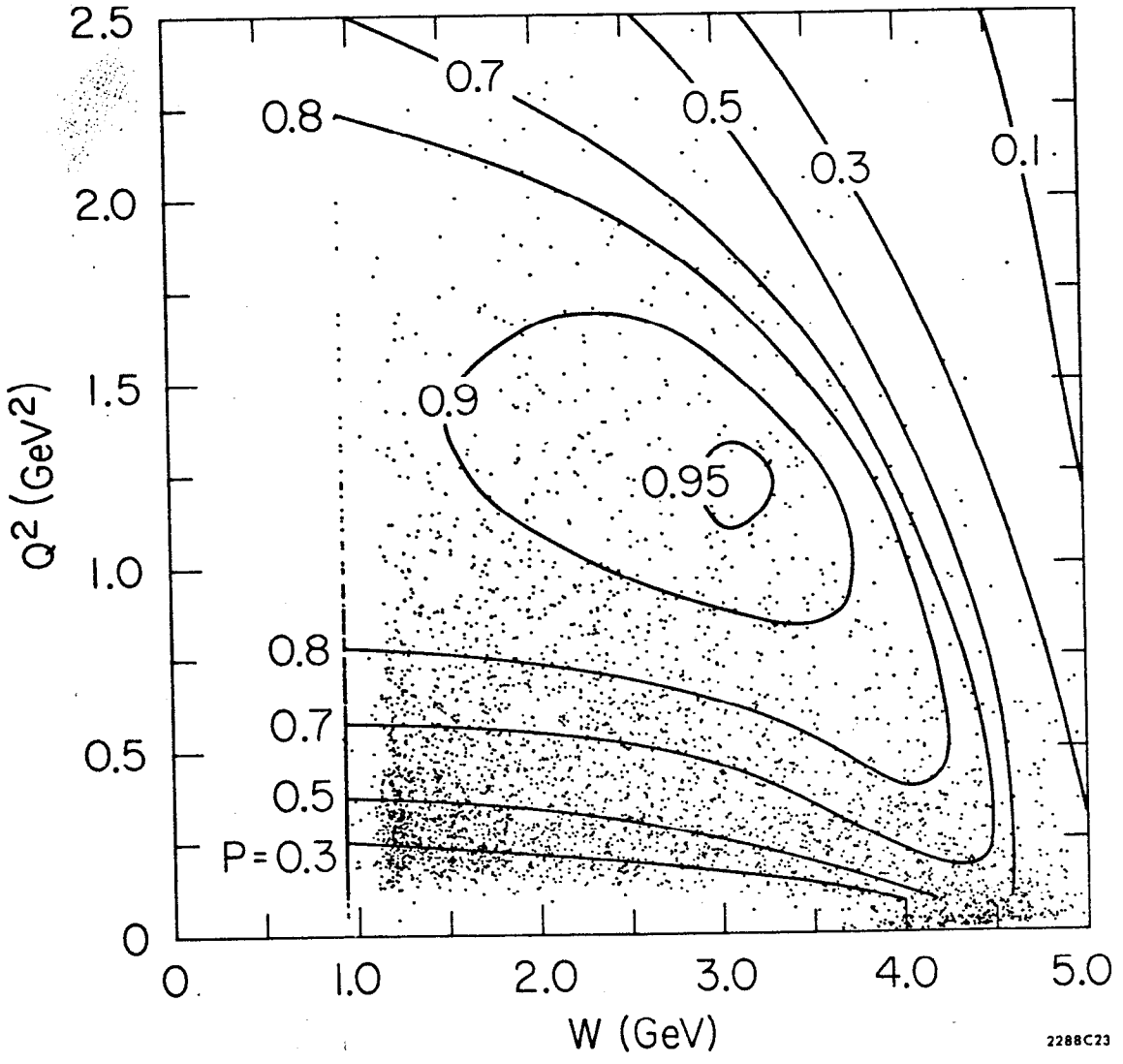


Fig.3a

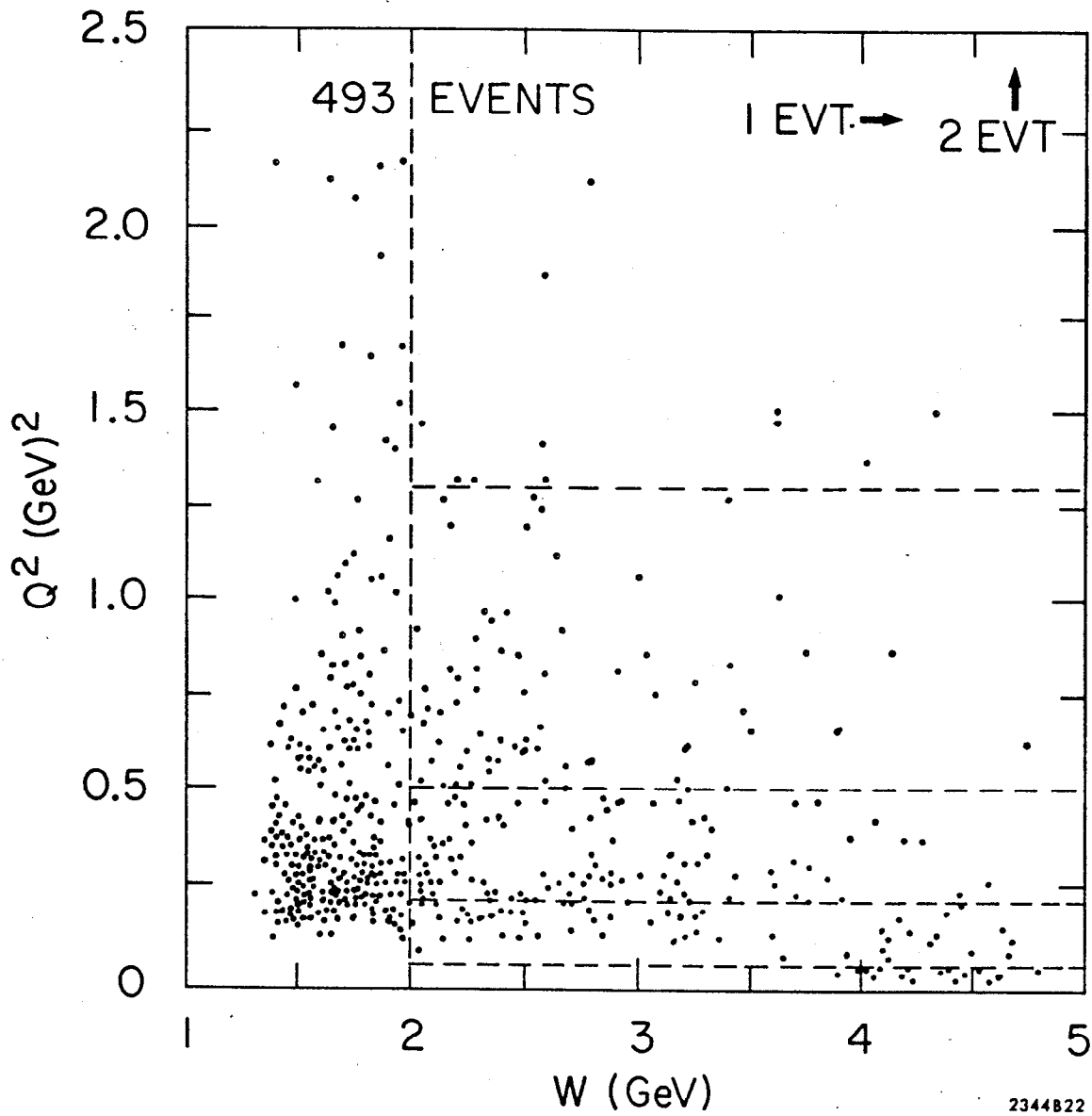
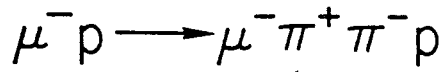


Fig. 3b

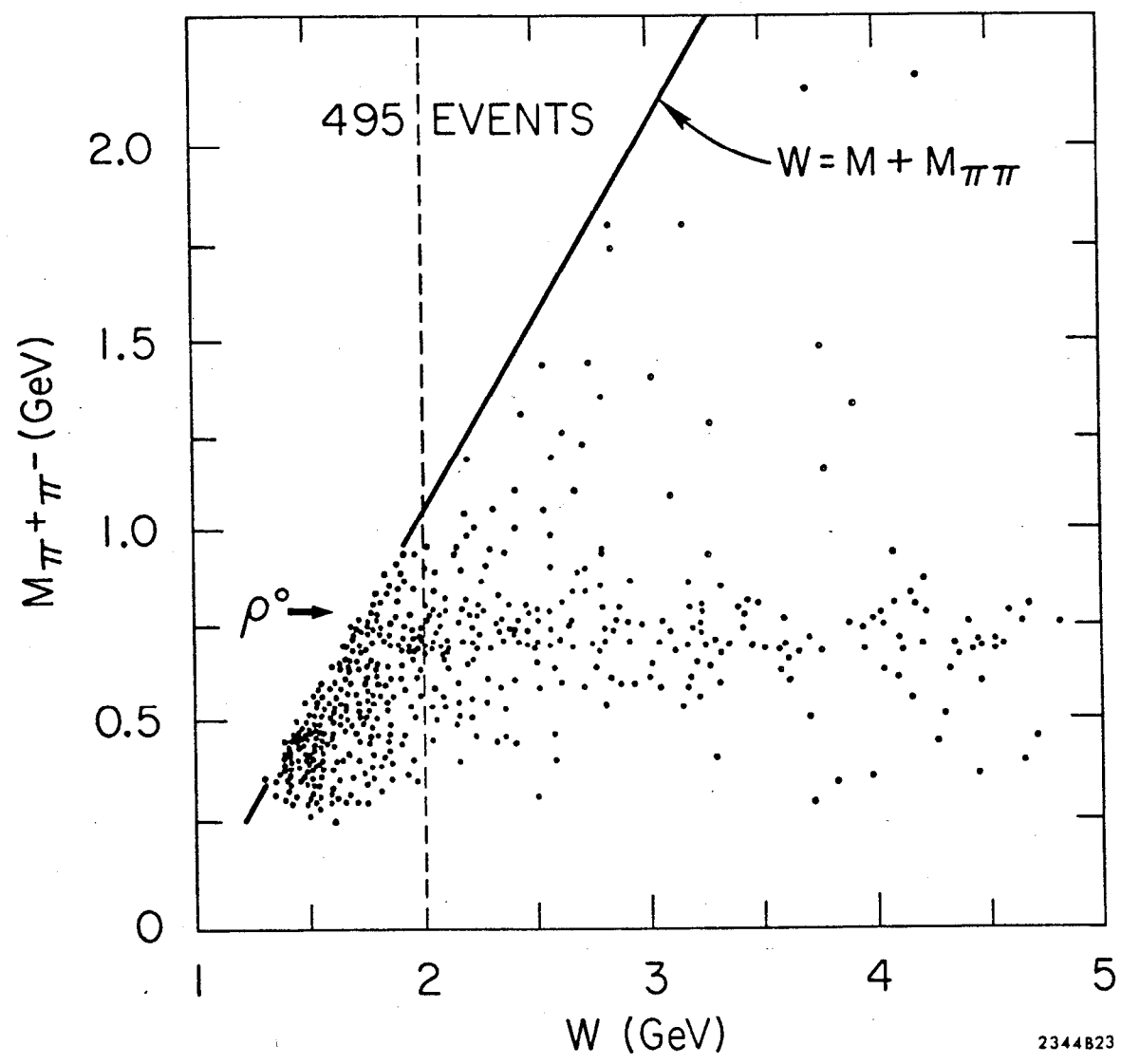
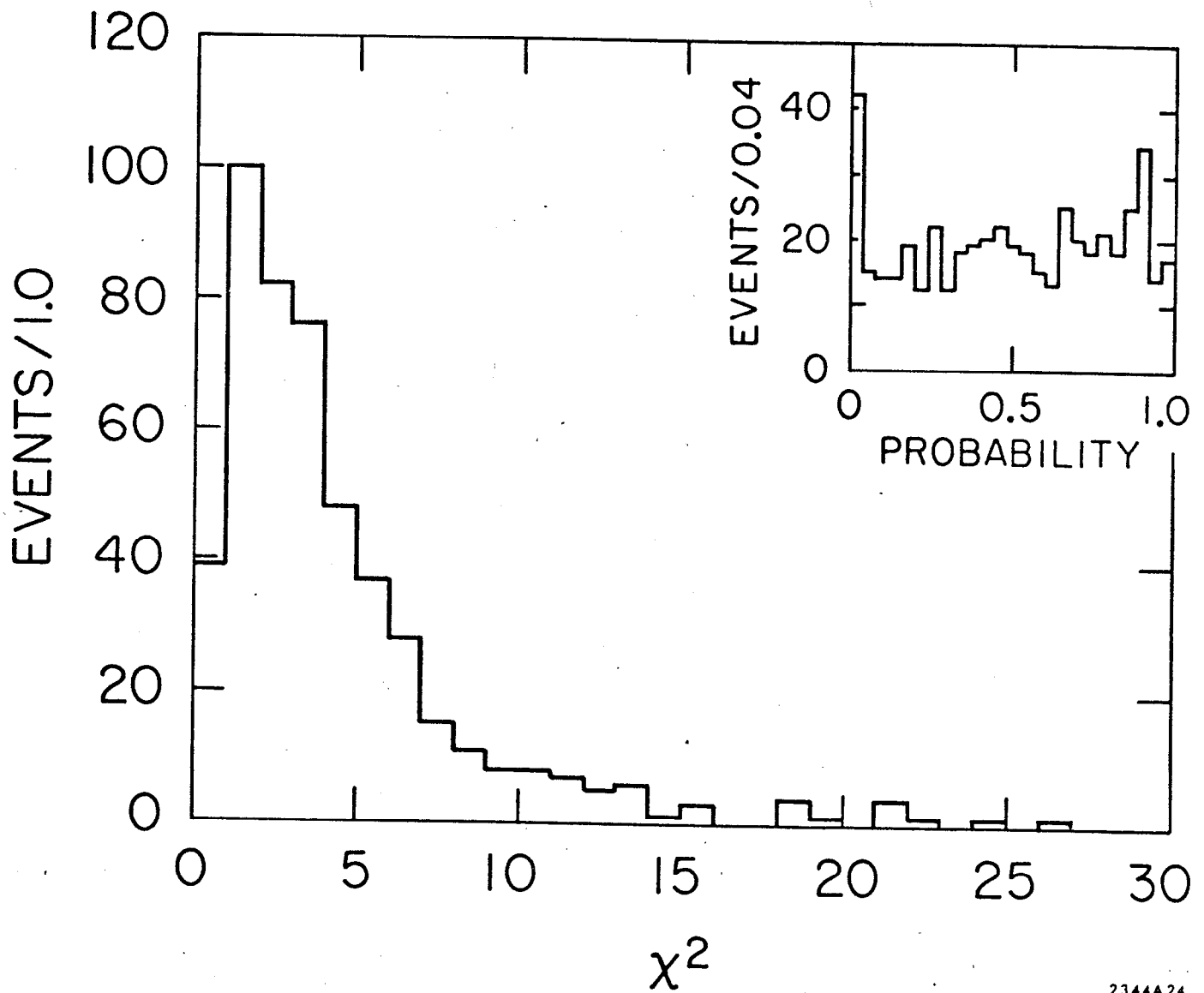
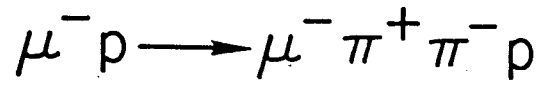


Fig. 3c



2344A24

Fig. 4

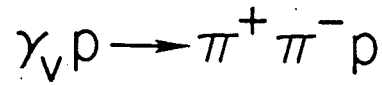
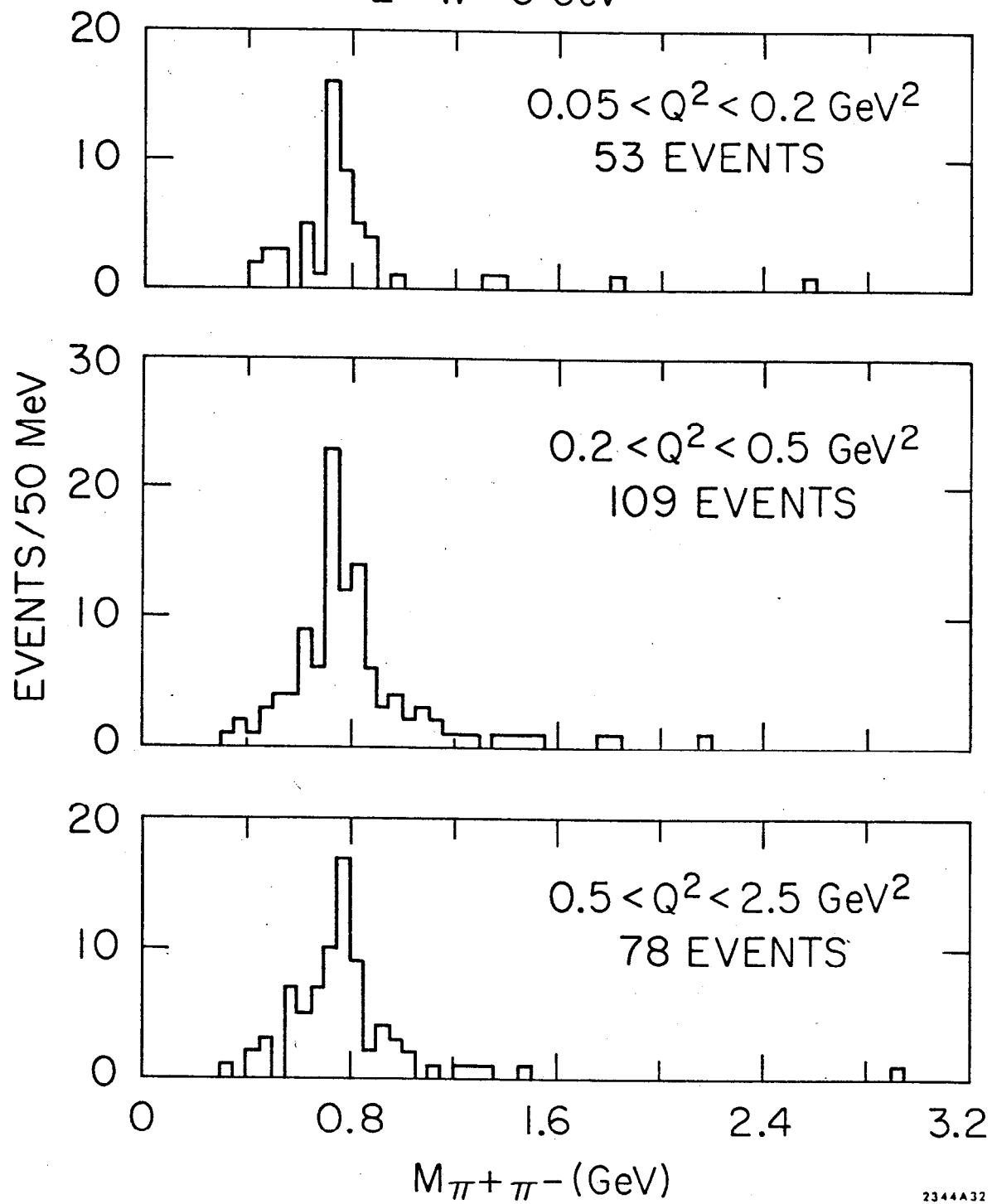
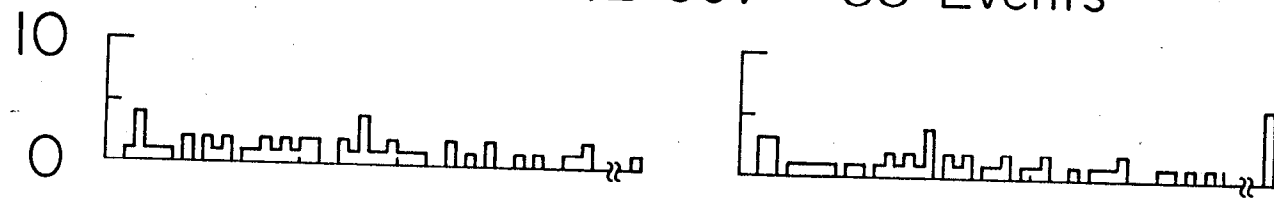

$$2 < W < 5 \text{ GeV}$$


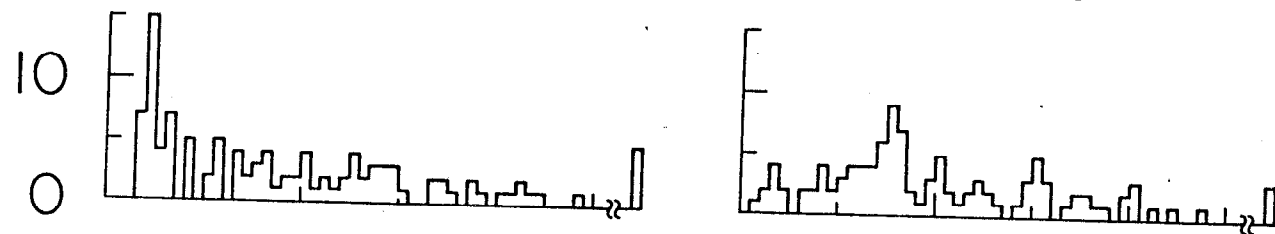
Fig 5a

$$\gamma_V p \rightarrow \pi^+ \pi^- p \quad W > 2 \text{ GeV}$$

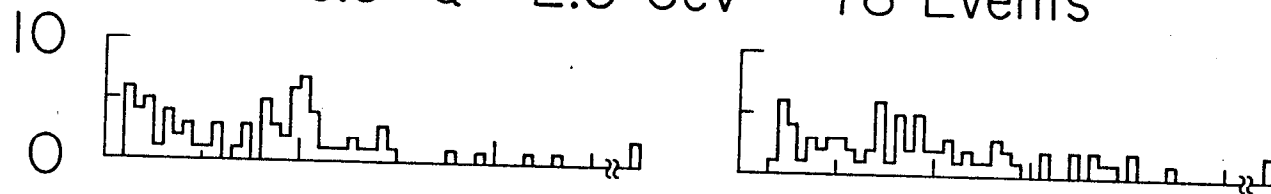
$0.05 < Q^2 < 0.2 \text{ GeV}^2$ 53 Events



$0.2 < Q^2 < 0.5 \text{ GeV}^2$ 109 Events



$0.5 < Q^2 < 2.5 \text{ GeV}^2$ 78 Events



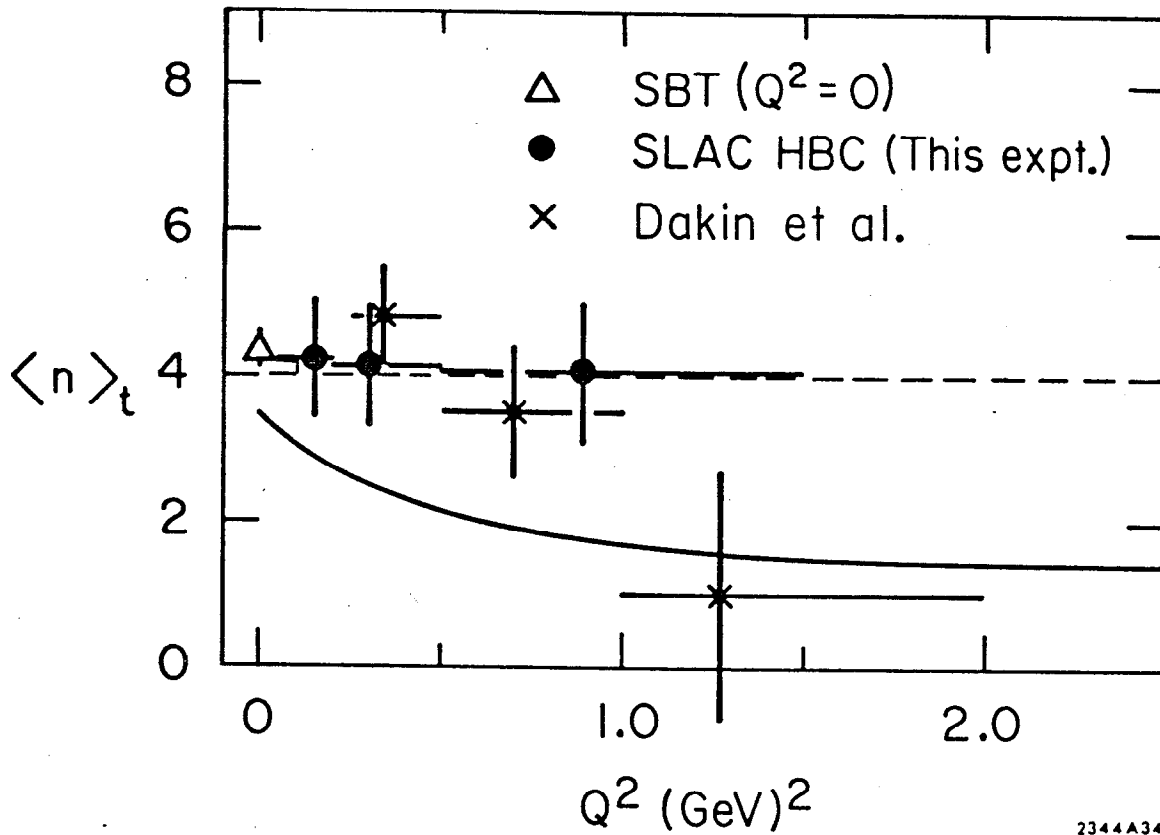
1.0 2.0 3.0
 $M_{\pi^+ p} \text{ (GeV)}$

1.0 2.0 3.0
 $M_{\pi^- p} \text{ (GeV)}$

2356810

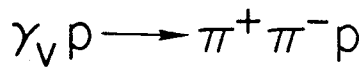
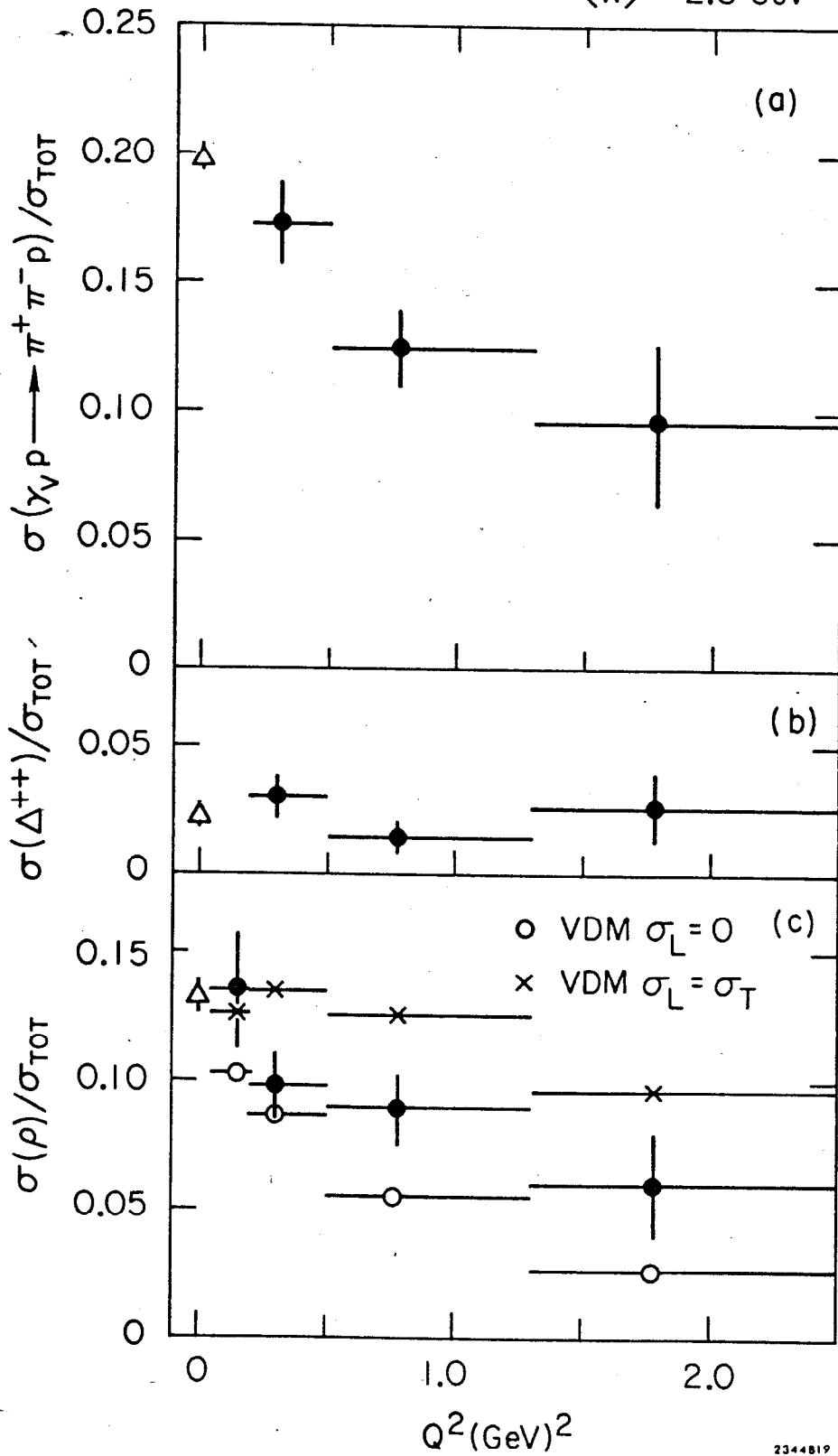
Fig. 5b

$\gamma p \rightarrow \rho^0 p$
 $2 < W < 5 \text{ GeV}$



2344A34

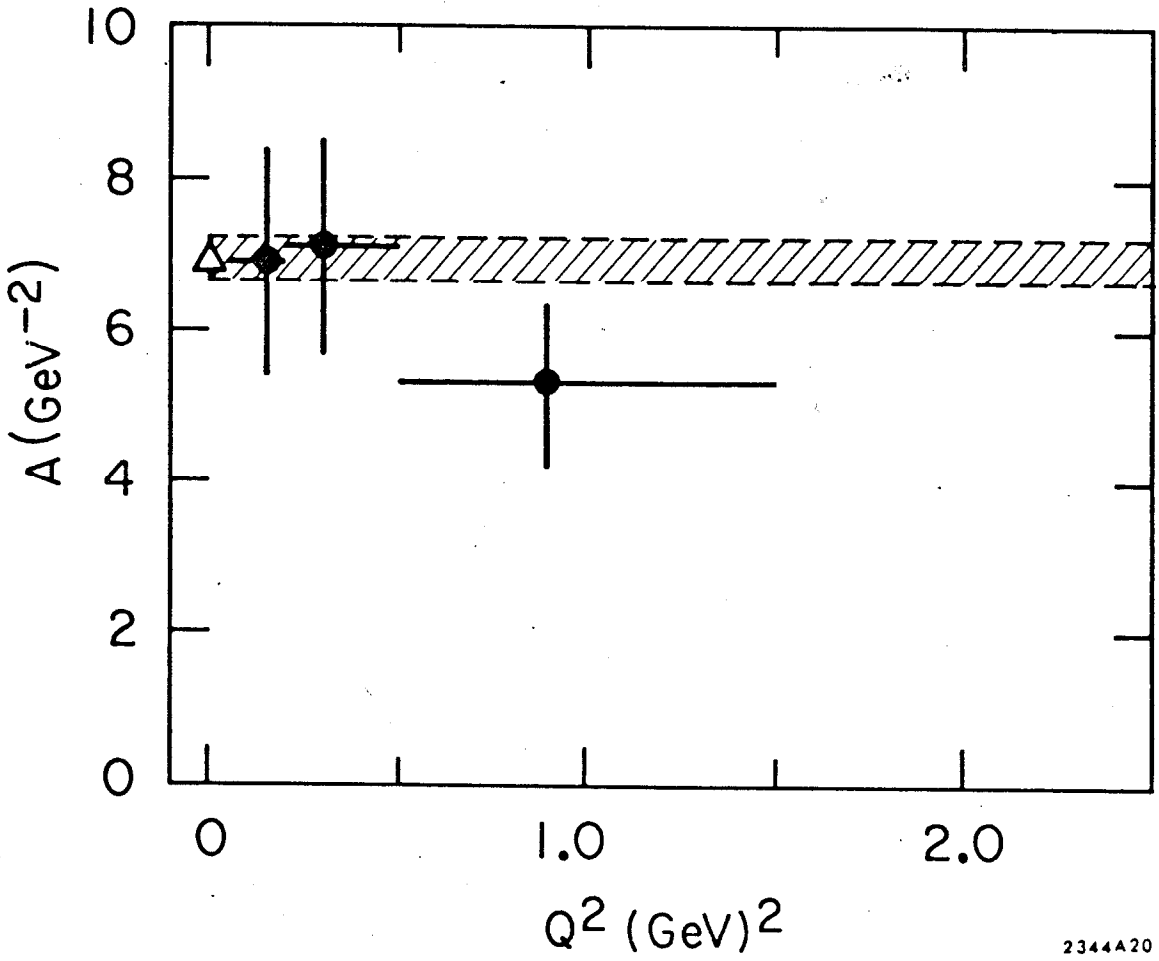
Fig. 6


 $2 < W < 5 \text{ GeV}$
 $\langle W \rangle \approx 2.8 \text{ GeV}$


2344819

Fig. 7

$\gamma p \rightarrow \rho^0 p$
 $2 < W < 5 \text{ GeV}$



2344A20

Fig. 8

SLAC HBC

$$\gamma_{\nu} p \rightarrow \pi^+ \pi^- p$$

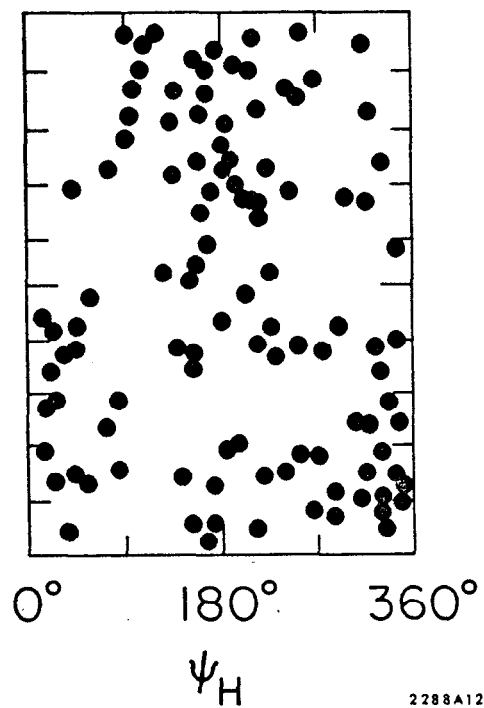
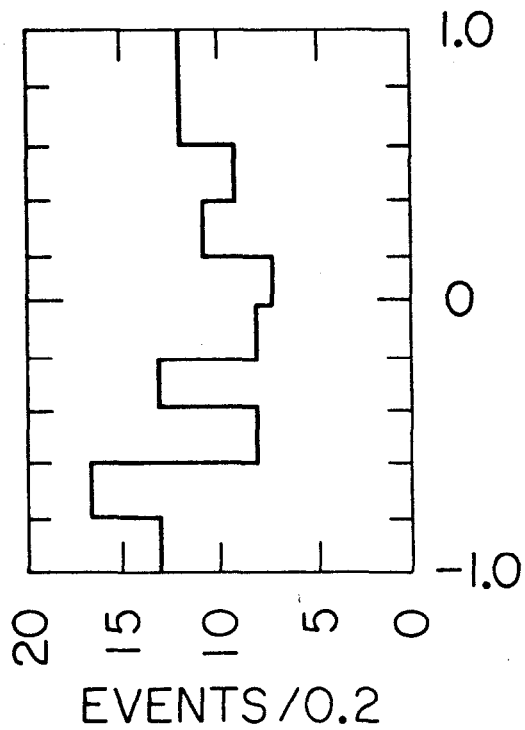
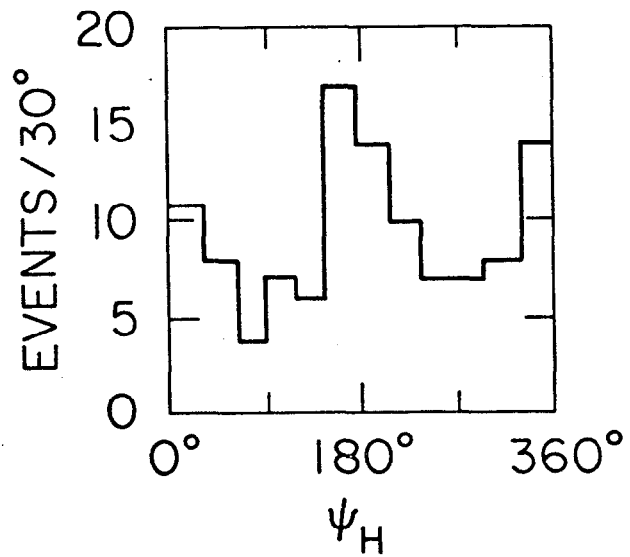
$$0.6 < M_{\pi^+ \pi^-} < 0.9$$

$$|t| < 0.6 \text{ GeV}^2$$

$$Q^2 > 0.15 \text{ GeV}^2$$

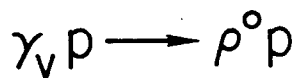
$$W > 2 \text{ GeV}$$

(109 Events)

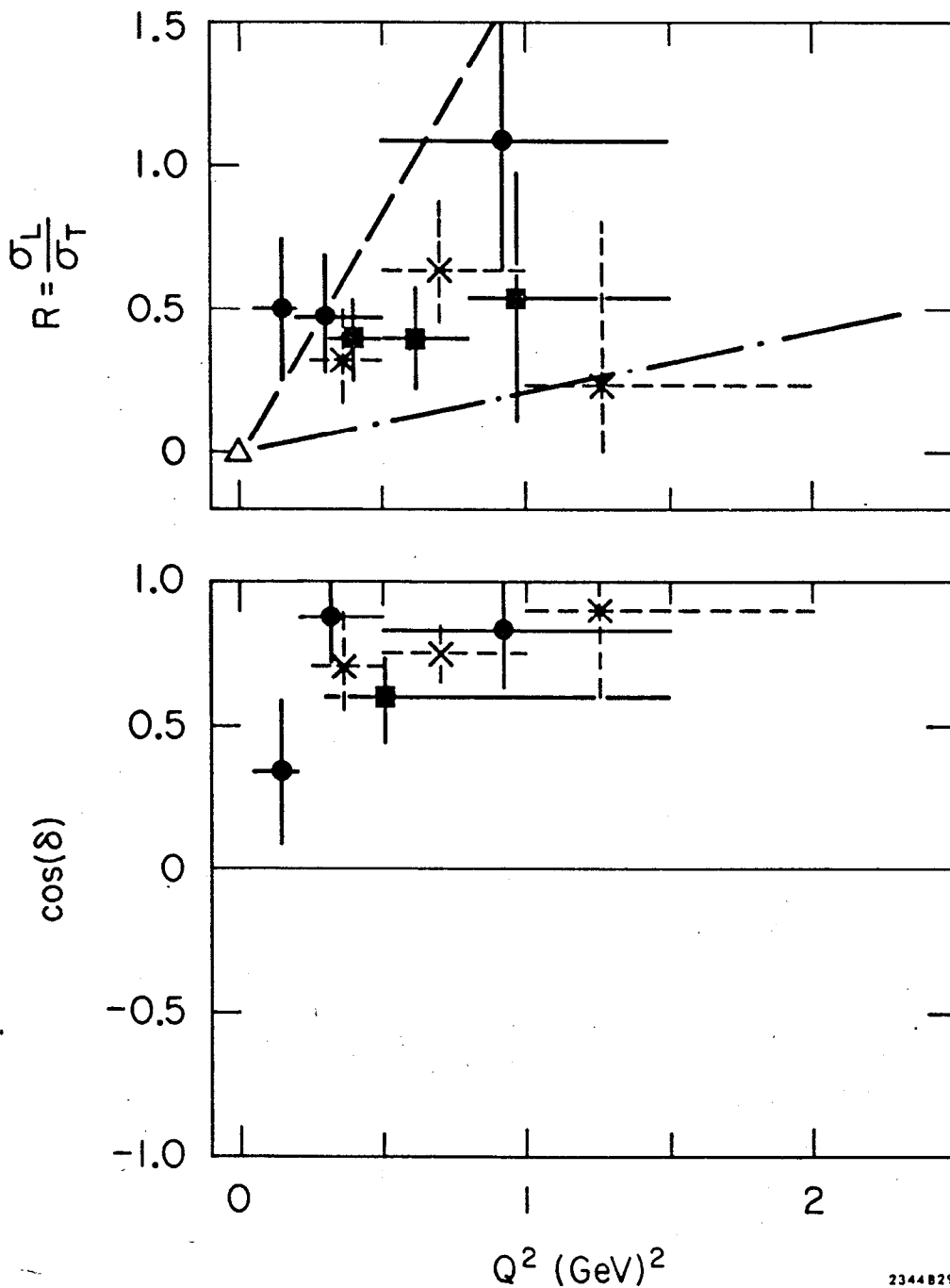


2288A12

Fig 9



- △ PHOTOPRODUCTION
- × Dakin et al. $\langle W \rangle = 4.5$ GeV
- Ballam et al. $\langle W \rangle = 2.8$ GeV (This expt.)
- Eckardt et al. $\langle W \rangle = 2.5$ GeV

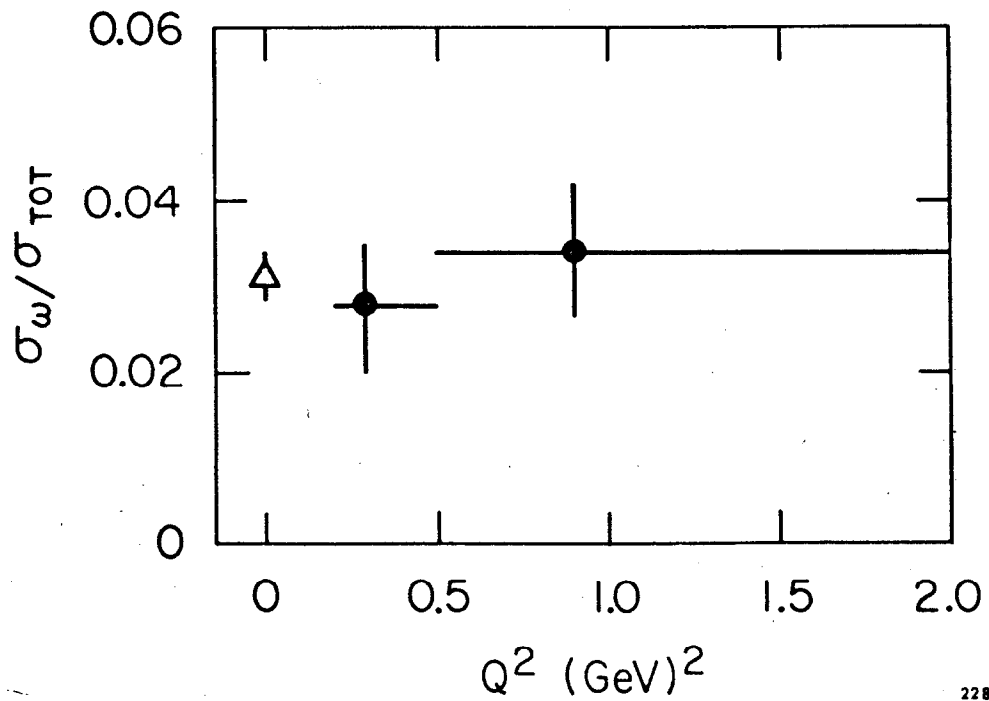
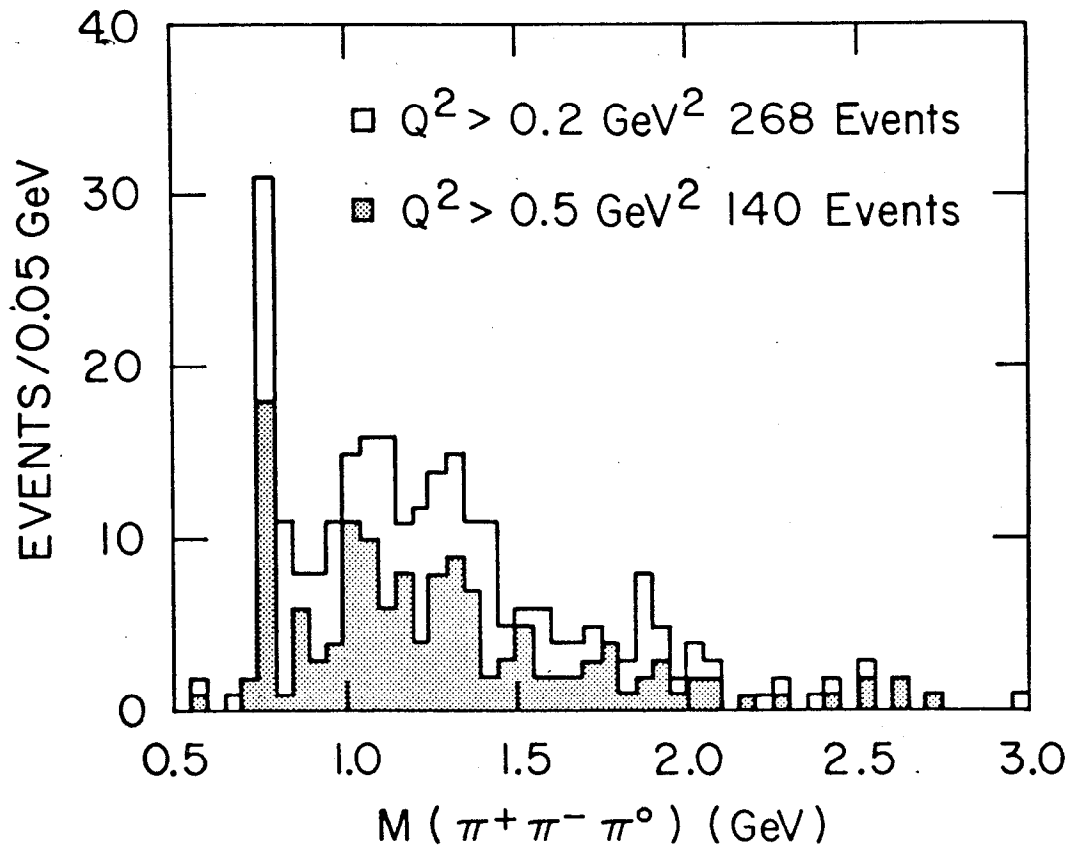


2344 B29

Fig. 10

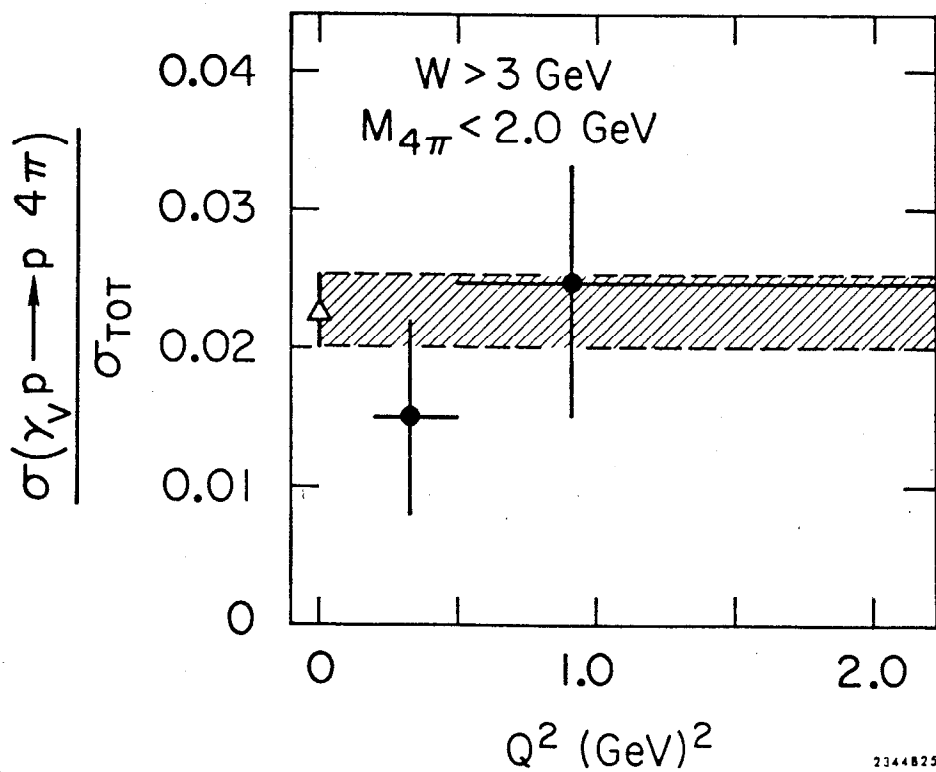
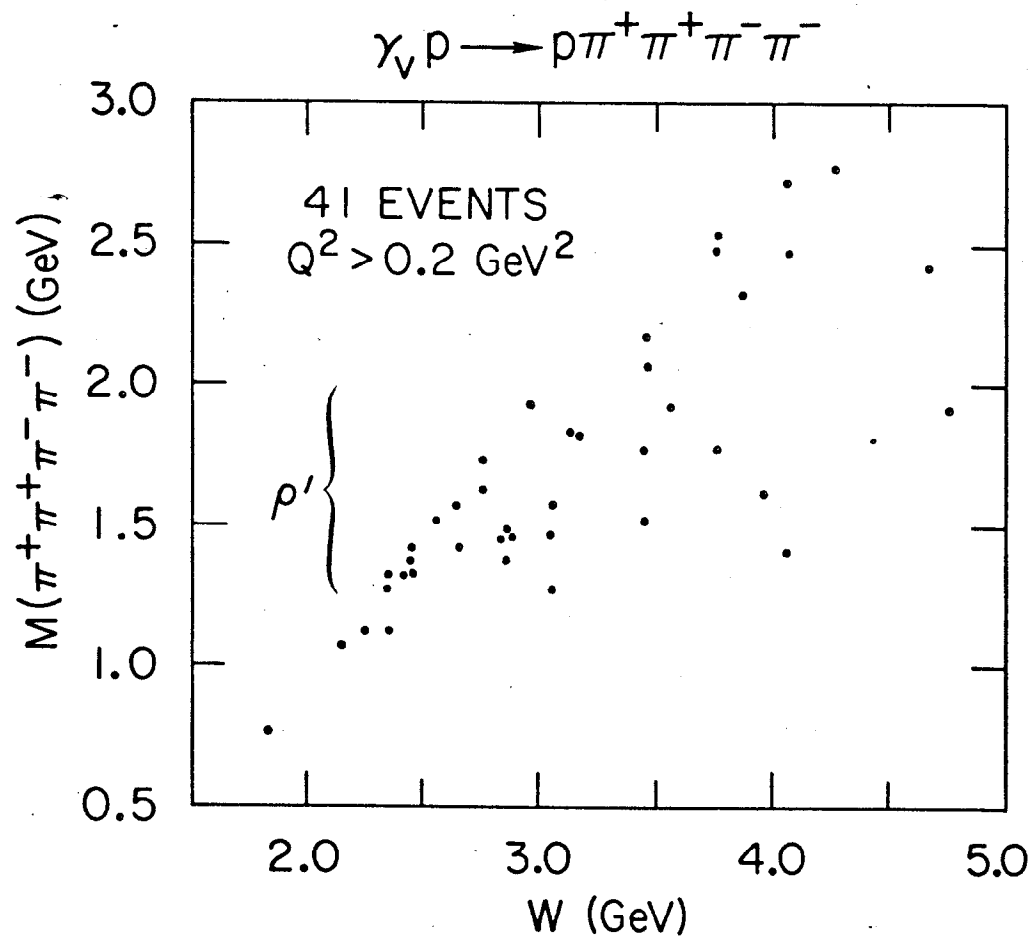
$$\gamma_V p \rightarrow p \pi^+ \pi^- \pi^0$$

$$W > 2.0 \text{ GeV}$$



2288A16

Fig. 11



2344825

Fig. 12

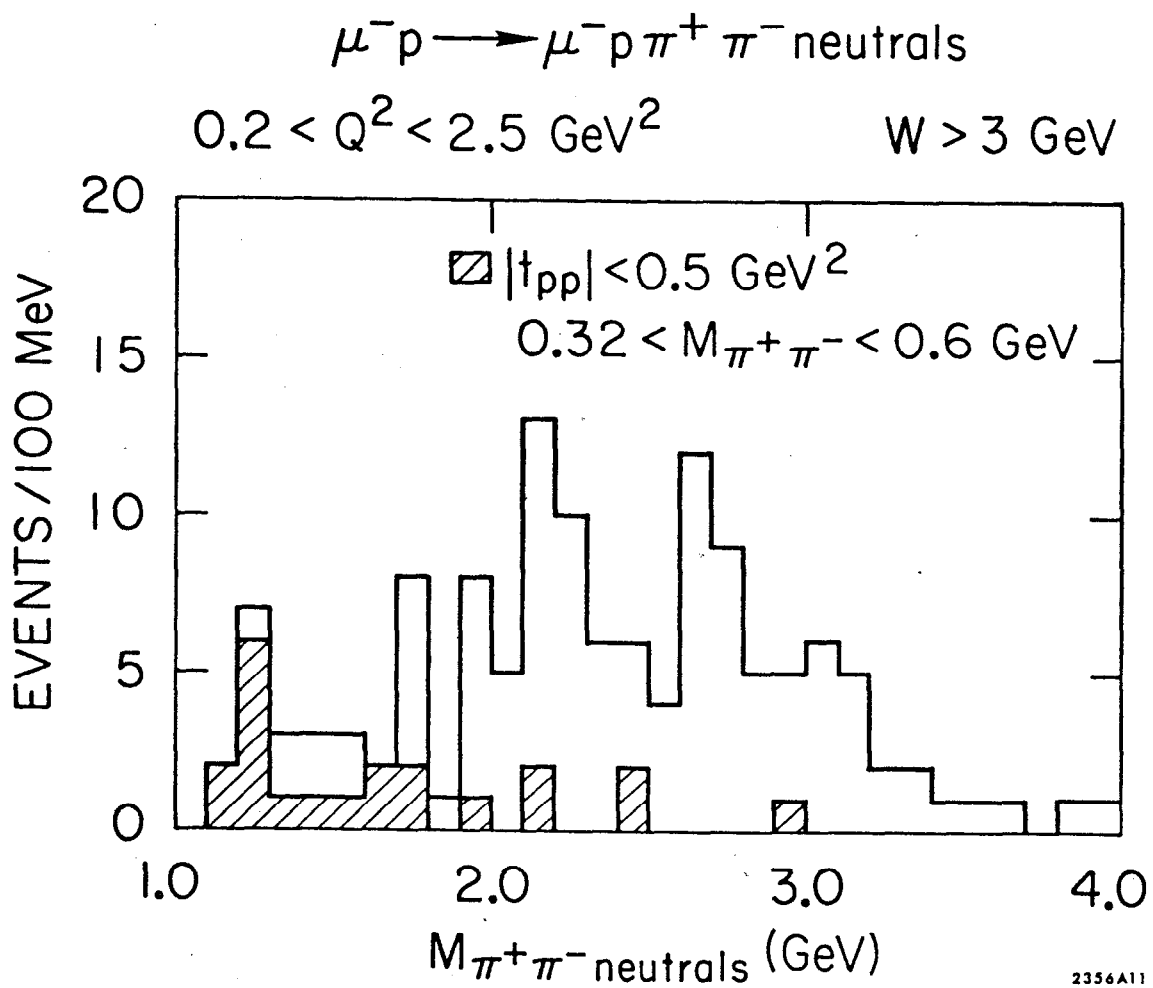


Fig 13